# CHAPTER 6

## Physical, Structural, Thermal and Electrical Properties of

## $x(AgI):(100-\mathrm{x})[30Ag_2O:(56B_2O_3+14P_2O_5)]$

## glass series

## 6.1 Introduction to the Glass Series:

The borophosphate glasses containing silver and doped with $AgI$ demonstrate remarkably elevated conductivities of $Ag^+$ ions, reaching approximately $10^{-2}\ S\ cm^{-1}$. The high conductivity is observed in these glasses, which is due to the presence of $\alpha - AgI$ structures within the glass. According to Magistris et.al; [1], who proposed that this conductivity is facilitated by the continuous transfer of $Ag^+$ ions from one iodine ion to another. The authors observed that $Ag^+$ ions rotate around $I^-$ ions, suggesting a mechanism for the conduction of charge. The introduction of salt via doping is mentioned as a means to increase the number density of charge carriers and enhance the available conduction pathways for these carriers. Doping refers to the intentional addition of impurities or foreign atoms into a material to modify its properties. In this case, the addition of salt increases the concentration of $AgI$, which in turn affects the diffusion rates of $Ag^+$ ions. An increase in the concentration of $AgI$ leads to a notable escalation in the rates of diffusion for $Ag^+$ ions. This implies that the higher the concentration of $AgI$, the more readily the $Ag^+$ions can move within the glass, contributing to increased conductivity [2]. The incorporation of $AgI$ into the glass matrix has been observed to primarily enhance the electrical characteristics of the glass. The properties of $AgI$-doped silver borophosphate glass is achievable by tuning the concentration of $AgI$ dopant and/or the composition of the glass system. Due to the fact that solid electrolytes are a type of material that exhibits a characteristic where the anionic or cationic constituents are not restricted to specific lattice sites but rather possess the ability to move freely throughout the structure [3]. The silver borophosphate glass system doped with $AgI$ exhibits significant potential for utilisation in diverse applications, such as electrochromic-based sensor devices and as solid electrolyte for supercapacitors and/or batteries. This chapter focuses on studying the effect of silver iodide ($AgI$) doping in silver borophosphate glass systems to investigate the migration of $Ag^+$ ions within the glass. An interesting observation has been noted that when the binary system consisting of two glass-forming oxides, $B_2O_3$ and $P_2O_5$, is used, it does not result in the formation of a glassy material. Instead, it leads to the formation of a crystalline compound called $BPO_4$. The structure of the $BPO_4$ compound is composed of tetrahedra of $BO_3$ and $PO_4$. This crystalline structure differs from the amorphous structure typically associated with glasses. It is important to note this distinction because it indicates that the formation of glassy materials in the specific binary system is not feasible. However, the authors highlight that borophosphate glasses, when doped with silver ions, exhibit exceptional ionic conductivity

along with thermal and electrochemical stability. This suggests that the introduction of silver ions into the borophosphate glass matrix enhances its ability to conduct ions, making it a promising option for solid-state batteries. The silver borophosphate glass system is characterized by the emergence of $BO_4$ tetrahedra, which leads to the formation of cross linking $B-O-P$ bridges. This ultimately results in the branching out of the borophosphate glass network in random manner, thereby rendering it more compact [4].

The present study involves the examination of the silver borophosphate glass system, characterized by $x(AgI):(100-\mathrm{x})[30Ag_2O:(56B_2O_3+14P_2O_5)]$ composition. The analysis mentioned in the statement reveals the presence of different structural groups, specifically $BPO_4$ and $BO_4$, within the material being studied. These structural groups possess favorable properties for ionic conduction, indicating their potential role in facilitating the movement of ions through the material. The structure of the glass skeleton, particularly influenced by the borate component of the network former, has been found to impact the fluctuations observed in the glass transition temperature with changing composition [5]. The borate constituent plays a significant role in modifying the structural arrangement of the glass, which in turn affects the glass transition temperature. In the specific case of the ternary glass system composed of silver borophosphate, the interactions between ions (coulombic interactions) are reduced. This reduction in coulombic interactions leads to the attainment of the lowest activation energy and the highest conductivity for the $Ag^+$ ions within the material. Reference [6] supports this finding by stating that the ternary glass system of silver borophosphate exhibits its minimum activation energy when the ionic coulombic interaction is at its lowest. This suggests that the reduced coulombic interactions contribute to enhanced ionic conductivity in this particular glass system. The formation of the $B-O-P$ link in the $M_2O-B_2O_3-P_2O_5$; $(M=Li/Na/Ag)$, glass system reveals a considerable preference for heteroatomic $B-O-P$ connections over homoatomic $P-O-P$ or $B-O-B$ bond formation [7]. According to the literature review, the ion conductivity and relaxation mechanism in the $M_2I$ doped borophosphate glass system has received scant attention to date in order to understand the transport mechanisms of $Li, Na,$ and $Ag$ (monovalent) ions in the metal oxide modified borophosphate glass system.

The research conducted by Suresh Kumar et al. [8] has reported an ionic conductivity on the order of $10^{-6}\,\mathrm{S\,cm^{-1}}$ for silver oxysalts doped with $CuI$. The specific material investigated in their study is not mentioned, but it is implied that the presence of $CuI$ as a dopant enhances the conductivity of the silver oxysalts. $AgI$ is considered a prototypical

material among metal halides. In $AgI$, the $Ag^+$ ions are surrounded by $I^-$ ions, which contributes to its high conductivity, particularly in the $\alpha - AgI$ phase [8], [9]. The $\alpha - AgI$ phase is known for its significant conductivity due to the arrangement of ions within the crystal structure. $AgI$ exhibits a solid-to-solid phase transition at approximately $420\ K\ (147\ °C)$. This transition is accompanied by a rapid increase in conductivity of more than three orders of magnitude. This behavior indicates a notable change in the mobility of ions, resulting in a substantial enhancement of conductivity.

It is worth noting that glasses that can accommodate the $AgI$ phase at ambient temperature demonstrate strong ionic conductivity. This is attributed to the presence of low activation barriers for ion migration within these glasses. The ability to maintain the $AgI$ phase in the glass structure even at room temperature allows for favorable ion mobility, leading to enhanced ionic conductivity. The hard and soft (Lewis) acids and bases (HSAB) theory is a chemical theory that helps to predict the reactivity of chemical species. The theory divides chemical species into two categories: hard acids-bases, and soft acids-bases. Hard acids and bases are those that are relatively small, have high charge densities, and are polarizable. Soft acids and bases are those that are relatively large, have low charge densities, and are not polarizable. The HSAB theory predicts that soft acids and bases will interact more strongly with each other than hard acids and bases. This is because soft acids and bases have similar properties, such as their size and charge density. In the case of $AgI$, the silver ion interacts more strongly with the iodide ion than it would with a smaller, more highly charged ion. This stronger interaction leads to the formation of a shallow potential well, which makes it easier for the silver ion to move through the glass. The addition of dopant salts, such as $LiCl$, to $AgI$-doped ionic glasses further enhances the ionic conductivity of the glass. This is because the dopant salts provide additional ions that can move through the glass. The dopant ions also help to break up the network of the glass, which makes it easier for the silver ions to move [10]. $Ag^+$ has a shallow potential well and is loosely associated with iodide in $AgI$ doped ionic glass, which softens the host glassy matrix and ion movement is supported by the high (cat-) ion decoupling. Deshpande et al;[11] illustrated that adding dopant salts like $LiCl$ to lithium borate and lithium borosilicate glasses causes the decoupling charge carriers ($Li^+$) to move from one NBO to the next in order to produce conduction. As a result, silver ions from $AgI$ can be decoupled, allowing them to quickly conduct cationic current even at low concentrations of $AgI$ through the openings created by anionic spheres in the glassy amorphous structure [9], [12], [13]. When $AgI$ is added to a

glass composition, it can influence the ionic conductivity of the material. In the study conducted by Minami et al; [14], they investigated the behavior of ionic conductivity in the $AgX$–$Ag_2O$–$B_2O_3$ glass system. According to their findings, the ionic conductivity in this glass system was reported to be approximately $10^{-2}\ S\ cm^{-1}$ at ambient temperature. This indicates that the glass exhibits relatively high conductivity, allowing for the movement of ions through the material. In the case of silver borophosphate glass, the maximum conductivity was observed at a temperature of 303 $K$ (~30℃), and it was approximately $10^{-5}\ S\ cm^{-1}$[1]. According to P. Sharma et al., the concentration of $AgI$ salt in the $AgI$–$Ag_2O$–$V_2O_5$–$TeO_2$ glass system increased ionic conductivity [15]. In glassy electrolytes, the number of NBOs (of the host matrix) and the number of mobile charge species mostly determine the ionic conductivity.

In the current system, the ionic salt $AgI$ has been varied within the composition of $x(AgI)$: $\{(100-x)[30\ Ag_2O$: $(56\ B_2O_3 + 14\ P_2O_5)]\}$, where $x = 0, 1, 3, 5$ and 7 $wt.\%$. Hence, investigating the systematic variations of $AgI$ salt in a highly firm borophosphate glassy system is an interesting and novel field of scope. The purpose of this study is to investigate the mechanism of ionic conduction in a silver-borophosphate glass system with a fixed ratio of glass former to modifier.

## 6.2 Experimental

### 6.2.1 Materials used

Raw materials such as boric acid ($H_3BO_3$), ammonium dihydrogen phosphate ($ADP - NH_4H_2PO_4$), silver oxide ($Ag_2O$) and silver iodide ($AgI$) were used for preparation of electrolyte materials.

### 6.2.2 Preparation method

In the present study, the glass sample composition with $x$ ranging from 0 to 7 $wt.\%$ in the glass series $x(AgI)$: $(100-\mathrm{x})[30Ag_2O$: $(56B_2O_3 + 14P_2O_5)]$ were prepared using conventional melt quench method. The ionic glass samples were made by taking the required amount of chemicals, properly mixing them in an agate mortar and pestle, and then preheating them at 450°C for 2 hours to eliminate the gases from the chemicals. The mixture was then heated at roughly 800°C for 6 hours before being quenched between two pre-cooled copper blocks. Depending on the proportion of $AgI$ in a glass composition, the

color of the prepared glass samples from transparent to pale yellow to orange. These samples were annealed in a furnace for an hour at 150°C to reduce thermal stress.

## 6.3 Results and discussion

### 6.3.1 Physical Characterization

Table 6.1 lists the physical data of glass system under consideration. Fig. 6.1(a) describes that density ($\rho$) increases from 3.99 $g/cc$ to 4.74 $g/cc$ when the $AgI$ salt content increases from 0 to 7 $wt.\%$. This may be related to the rise in iodide ion molecular weight (126.9045 $g/mole$) in $AgI$. In the study, the molar volume ($V_m$) of the glass structure, as shown in Fig. 6.1(a), was investigated, specifically in relation to the addition of $AgI$ (silver iodide). The researchers observed that initially, as the concentration of $AgI$ increased, the molar volume of the glass increased from 32.1647 $cc/mole$ to 40.8892 $cc/mole$. This indicates that the addition of $AgI$ led to an expansion or increased spacing within the glass structure. However, beyond a certain point, when the glass contained 3, 5, and 7 $wt.\%$ of $AgI$, the molar volume started to decrease. This suggests that further addition of $AgI$ caused a compaction or reduction in the spacing between atoms or molecules within the glass structure. Additionally, the study also investigated the oxygen packing density (OPD) of the glass samples. OPD refers to the density or arrangement of oxygen atoms within the glass structure. For the ABP5 sample, the addition of $AgI$ resulted in a decrease in OPD from 83.3210 $mol/l$ to 67.2836 $mol/l$, indicating a reduction in the packing density of oxygen atoms. On the other hand, for the sample labeled ABP7, the addition of $AgI$ caused an increase in OPD, implying an enhancement in the packing density of oxygen atoms. Regarding the molar volume of oxygen ($V_O$), the study observed that for the undoped sample (without $AgI$) and up to 1 $wt.\%$ doped sample, the molar volume increased. However, for the subsequent samples, the molar volume of oxygen gradually decreased. It is noted that the presence of modifier oxide and additive halide facilitates the liberation of $Ag^+$ ions. This can be observed in Fig. 6.1(b), where there is a gradual increase in the effective count of cations released for conduction. This increase in the number of cations available for conduction has the potential to enhance the overall conductivity of the glass.

Furthermore, Fig. 6.1(c) shows that the ABP5 sample code has the highest concentration of cations at the Fermi energy level ($E_f$). The Fermi energy level represents the highest occupied energy state at absolute zero temperature and is an indicator of the availability of charge carriers. In this case, the higher concentration of cations at the Fermi energy level

suggests an increase in either defect energy states or free charge carriers within the glass structure. The rise in defect energy states can be attributed to the incorporation of $Ag^+$ ions and the interaction between the modifier oxide and additive halide. These defects or energy states can act as additional sites for charge carriers, contributing to the overall conductivity of the glass.

Alternatively, the increase in free charge carriers can be a result of the liberated $Ag^+$ ions, which can act as mobile charge carriers within the glass structure. The presence of a higher concentration of cations at the Fermi energy level implies a larger number of mobile charge carriers, which can enhance the conductivity of the glass as previously reported [16]. The ionic conductivity is influenced by the carrier concentration and mobility of mobile ions, which results in a boost in the mobility of the charge carriers possessing the minimum activation energy for ion migration.

***Table 6.1**: Physical parameters of the silver borophosphate glass system doped with $AgI$.*

| Sample code | Network former ($B_2O_3 - P_2O_5$) | Network modifier ($Ag_2O$) | Additive ($AgI$) | Density $\rho$ ($g/cc$) | Molar volume $V_m$ ($cc/mole$) | Oxygen Packing Density OPD ($mole/l$) | Oxygen Molar Volume $V_O$ ($cc/mole$) | cation concentration $N_{oxide}$ $x\ 10^{21}$ /cc | cation concentration $N_{iodide}$ $x\ 10^{21}$ /cc | Total cation concentration$N$ $x\ 10^{21}$ /cc | $N$ at $E_f$ concentration $x\ 10^{21}/(eV)\ cc$ |
|---|---|---|---|---|---|---|---|---|---|---|---|
| | ($wt.\%$) | | | | | | | | | | |
| **$ABP0$** | 70 | 30 | 0 | 3.99 | 32.16 | 83.32 | 12.00 | 5.62 | - | 5.62 | 1.60 |
| **$ABP1$** | 69.3 | 29.7 | 1 | 4.20 | 40.89 | 64.89 | 15.41 | 5.80 | 0.20 | 5.99 | 2.08 |
| **$ABP3$** | 67.9 | 29.1 | 3 | 4.28 | 40.41 | 66.81 | 14.97 | 5.70 | 0.60 | 6.29 | 2.68 |
| **$ABP5$** | 66.5 | 28.5 | 5 | 4.60 | 37.84 | 67.28 | 14.86 | 5.91 | 1.05 | 6.95 | 3.39 |
| **$ABP7$** | 65.1 | 27.9 | 7 | 4.74 | 28.66 | 86.98 | 11.50 | 5.86 | 1.49 | 7.34 | 3.37 |

### 6.3.2 Thermal Characterization

The phenomenon of mobile ion migration in FIC glasses is attributed to the dissociation of cations from the rigid glass network. In other words, the presence of mobile ions in the glass is a result of cations becoming detached from the structural framework of the glass [17]. To determine the decoupling index, which indicates the degree of dissociation between mobile

ions and the glass network, knowledge of the glass transition temperature ($T_g$) is sufficient [18]. The glass transition temperature is a critical parameter that is directly influenced by the composition of glasses. In the specific system being studied, the incorporation of $AgI$ into the glass composition leads to a slight decrease in the glass transition temperature. Initially, the $T_g$ falls from $423\ K$ to $412\ K$ with the addition of $AgI$ up to $5\ wt.\%$. However, for the ABP7 sample, there is an upward trend, and the glass transition temperature increases to $420\ K$. The current study supports the result previously reported by Angell [18], indicating that the introduction of $AgI$ causes a gradual reduction in the glass transition temperature. This suggests that the incorporation of $AgI$ affects the mobility and dissociation of cations within the glass structure, leading to changes in the glass transition behavior [18]. This phenomenon is attributed to the disruption of the glass structure and the consequent modification of the structure by cations. Subsequently, the glass transition temperature experiences an elevation to $420\ K$ in the case of the ABP7 specimen. The displacement of the $T_g$, as depicted in Fig. 6.1(d), in the current system towards the lower temperature range can be explained by a reduction in the rigidity of the glass structure and an increase in the presence of non-bridging oxygen within the structure**.**

At a concentration of $7\ wt.\%$ of $AgI$, it is possible that the observed increase in structural rigidity is attributable to an elevation in the glass transition temperature. J Shelby demonstrated that the glass structure is altered not only by modifiers but also by the involvement of additive $AgI$ [19]. It is observed that the introduction of a higher number of non-bridging oxygen (NBO) species within the glass structure leads to a decrease in the viscosity of the glass. Non-bridging oxygen atoms are oxygen atoms that are not bonded to two network-forming atoms, resulting in the disruption of the glass network and increased mobility. Fig. 6.1(e) illustrates the profile of the decoupling index with respect to temperature and glass composition. The decoupling index is a parameter that indicates the concentration of ions that have been decoupled or dissociated from the parent glass matrix. In other words, it represents the degree of mobility and dissociation of ions within the glass. The study suggests that as the number of NBOs increases, the decoupling index also increases, indicating a higher concentration of ions that have been decoupled from the glass matrix. This is likely due to the disruption of the glass network by the NBOs, enabling greater ion mobility within the glass structure.

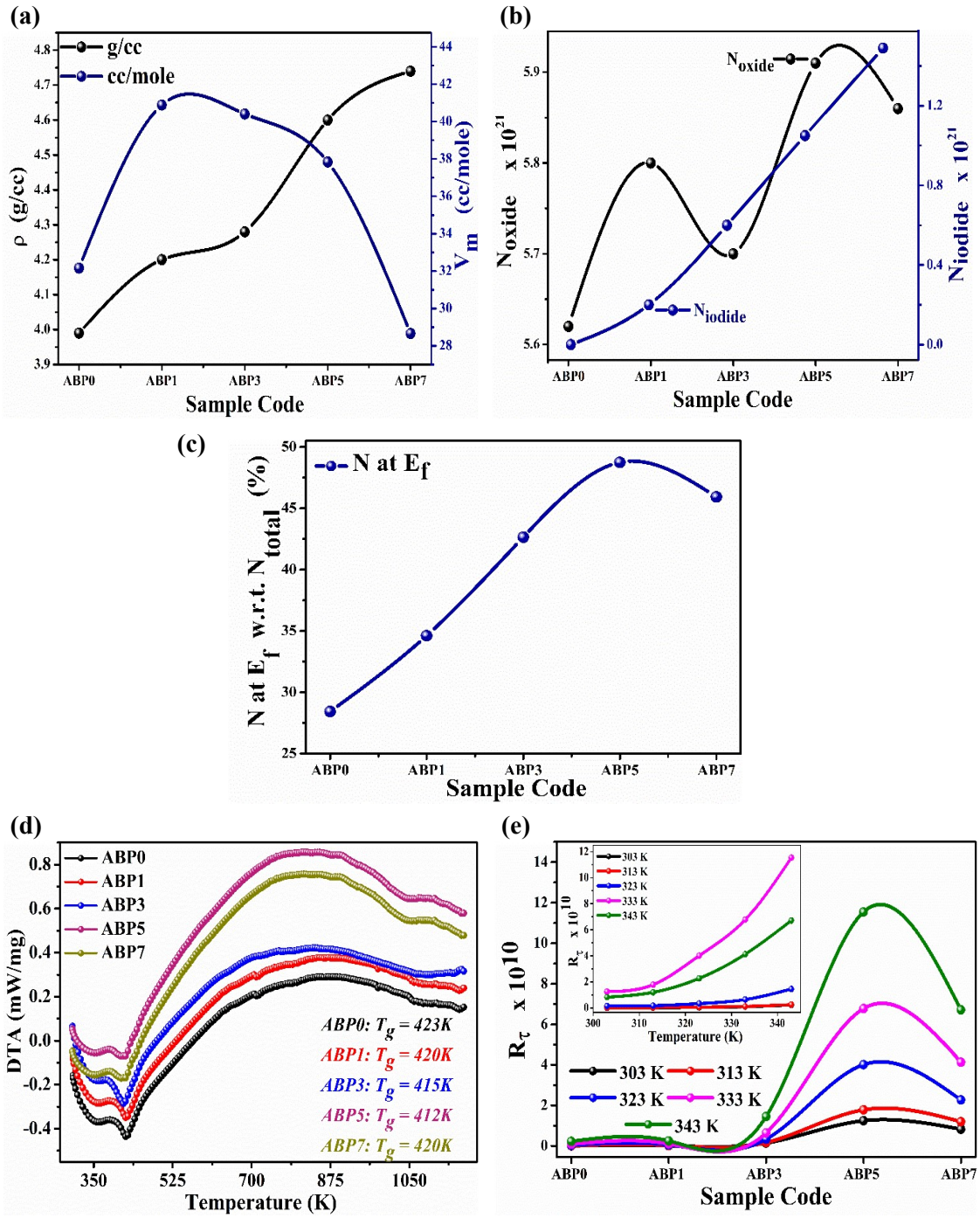


***Figure 6.1**: (a) ρ and $M_v$, (b) $N_{oxide}$ and $N_{iodide}$ (c) % of $N_{total}$ at $E_f$, (d) $T_g$, and (e) $R_\tau$ (inset: $R_\tau$ vs temperature), as a function of LBP glass series samples.*

The current investigation reveals that the decoupling index experiences an increase up to 5 $wt.\%$ of $AgI$ incorporation in a glass composition, followed by a subsequent decrease beyond this threshold [14].

### 6.3.3 Structural Characterization

#### a) X-ray Diffraction study

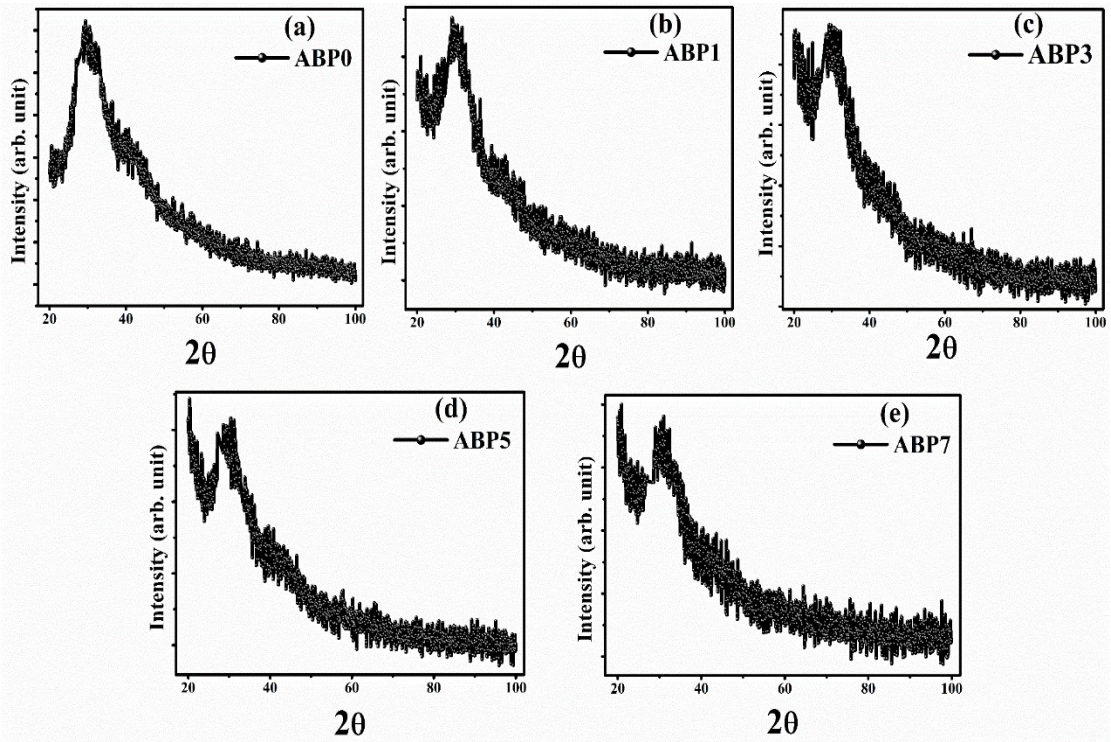


***Figure 6.2**:(a-e) X-ray diffraction patterns of all glassy electrolyte samples from ABP0 to ABP7, respectively.*

The X-ray diffraction patterns of the prepared glassy electrolytes, depicted in Fig. 6.2(a-e), exhibit a wide peak at approximately $2\theta \sim 29°$ and absence of discernible crystalline peaks throughout the spectra, indicating the fully amorphous character of the electrolyte samples that were prepared. The incorporation of $AgI$ into the samples did not result in the emergence of any novel peak or phase. However, a marginal displacement of the peak was observed in ABP5 within the range of $2\theta \sim 27° - 28°$. The absence of a distinct peak in the spectra indicates that $AgI$ has been fully dissolved into an amorphous phase.

#### b) Fourier Transform Infrared (FT-IR) Spectroscopy study

The effect of $AgI$ salt on the vibrational bond lengths and molecular structure is analyzed using Fourier Transform Infrared (FTIR) spectroscopy which is a technique that measures the absorption of infrared light by a sample, providing information about the molecular composition and functional groups present. The FTIR absorption spectra were recorded within the wave number range of 400 $cm^{-1}$– 1700 $cm^{-1}$, as shown in Fig. 6.3. The wave number represents the reciprocal of the wavelength of the infrared light and is measured in units of $cm^{-1}$. This range of wave numbers corresponds to specific quantized frequencies at which the molecular structure undergoes oscillation. Table 6.2, provided in the study,

presents the wave number of the peaks observed in the FTIR spectrum, along with their corresponding vibrational modes and assigned infrared (IR) bands. Vibrational modes refer to the specific types of molecular vibrations that occur within the compound.

In the mentioned study, the researchers analyzed the FTIR spectrum and observed specific peaks at various wave numbers. The behavior of these peaks was studied in relation to the addition of $AgI$ in the system. Here are the observations made regarding the peak intensities and their corresponding wave numbers:

1. Peaks at 430 $cm^{-1}$ and 470 $cm^{-1}$: The intensity of these peaks decreases with the addition of $AgI$ in the system. The specific vibrational modes or bond assignments for these peaks are not mentioned.
2. *P-O-P* bending peak at 530 $cm^{-1}$: This peak does not show any significant change with the addition of $AgI$.
3. *B-O-B* bending peak: This peak gradually shifts from 703 $cm^{-1}$ to 670 $cm^{-1}$ with the addition of $AgI$. The shift indicates an increase in the angular displacement of the *B-O-B* bond. [20], [21], [21].
4. Symmetric stretching of $P-O^{-}$: The peak intensity associated with the wavenumber range of 1080 $cm^{-1}$– 1090 $cm^{-1}$ as reported by Kabi et al; and Rao et al; [22], [23] increases with the addition of $AgI$ up to 5 $wt.\%$. However, for the ABP7 sample, a reduction in peak intensity is observed.
5. Emergence of a new absorption peak at 1225 $cm^{-1}$: The presence of this peak for $AgI$ up to 3 wt.% indicates an increase in the number of $P-O^{-}$ molecules and an increase in peak intensity. This peak corresponds to the asymmetric vibration of the $PO_2$ group.
6. Infrared band attributed to the asymmetric vibration of $P=O$: This band, observed at approximately 1385 $cm^{-1}$ in the ABP0 sample, experiences a gradual redshift and reaches 1349 $cm^{-1}$ for the ABP7 sample. This shift in wave number indicates a change in the vibrational behavior of the $P=O$ [24] bond within the phosphate chain.

These observations provide insights into the changes in peak intensities and wave numbers associated with specific vibrational modes and bond types within the glass system as a result of the addition of $AgI$. They help in understanding the modifications in the molecular structure and bonding induced by $AgI$ incorporation.

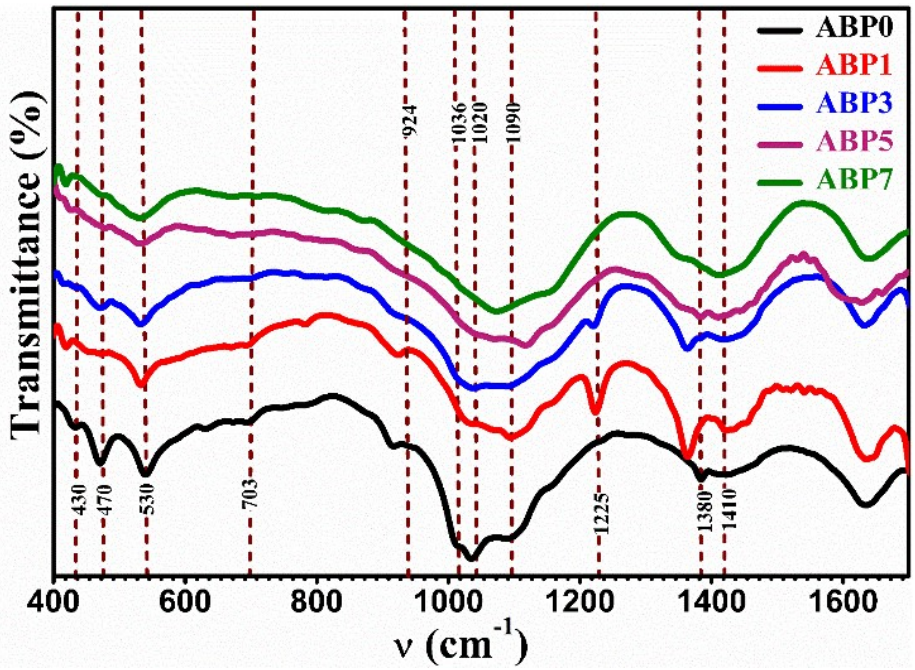


***Figure 6.3**: FTIR spectra of LBP glass series between 400 $cm^{-1}$ to 1700 $cm^{-1}$ wave number.*

The concentration of $AgI$ is observed to have a decreasing effect on the intensity of the mentioned peak. The introduction of $Ag^{+}$ ions derived from $AgI$ through interstitial means has been observed to have an influence on the $P = O$ bond within the system, resulting in an increase in bond length. The stretching of the $P = O$ bond is anticipated to result in a shift towards a lower wave number in the IR frequency. The absorption band located at 1410 $cm^{-1}$ in all of the glass specimens pertains to the asymmetric stretching of the trigonal borate unit [25]. This band remains unaltered in all of the glass specimens, indicating that the structure of the trigonal borate unit is not affected by the addition of $AgI$. The vibrational frequency of the $P - O - H$ bond is observed to occur at approximately 1638 $cm^{-1}$ in ABP0 [24], [26]. This peak is ascribed to the presence of water absorbed during the preparation of $KBr$ pellets for infrared spectroscopy measurements. The presence of water in the glass structure is not surprising, as water is a common impurity in glass. The frequency of the $P - O - H$ bond is also subject to gradual shifts upon the incorporation of $AgI$ into the glass structure. This shift is likely due to the interaction of the $AgI$ with the water molecules in the glass structure.

The interaction of $AgI$ with water molecules can cause the water molecules to become more tightly bound to the glass structure, which can lead to a decrease in the vibrational frequency of the $P - O - H$ bond.

***Table 6.2**: Band positions and assignments of IR bands of present glass system.*

| Wavenumber ($cm^{-1}$) | Mode of Vibration | Assignment of IR band | Reference |
|---|---|---|---|
| ~430 – 470 | ($\delta_s$) | O-P-O bonds (of $PO_4^{3-}$ group) and O-B-O bending bond | [24] |
| ~530 | ($\delta_s$) | O=P-O bonds due to deformation mode of $PO^-$ | [24], [26] |
| ~670 – 730 | ($\delta_s$) ($\nu_s$) | B-O-B linkage in various borate unit and P-O-P bridge | [20], [25], [28] |
| ~924 | ($\nu_s$) | P-O-P chain of $PO_4^{3-}$ group | [24], [26], [27] |
| ~1020 – 1030 | ($\nu_{as}$) ($\nu_s$) | B-O bond of $BO_4^{3-}$ tetrahedron unit and $PO_3$ unit | [14], [21], [26], [29], [30] |
| ~1090 – 1120 | ($\nu_{as}$) | P-$O^-$group of orthophosphate ($PO_4^{3-}$) | [26], [29], [30] |
| ~1130 – 1160 | ($\nu_{as}$) | $BO_3^-$ of penta borate unit | [25], [28] |
| ~1225 | ($\nu_{as}$) | Metaphosphate $(PO_2)^-$ group | [26], [27] |
| ~1330 – 1360 | ($\nu_s$) | pyro and ortho borate groups in $BO_3$unit | [14], [25] |
| ~1385 – 1339 | ($\nu_{as}$) | P=O in NBO atom of phosphate chain | [24] |
| ~1410 – 1420 | ($\nu_{as}$) | Borate triangle unit ($BO^-$) | [25] |
| ~1450 – 1460 | ($\nu_{as}$) | B-O stretching of triangle $BO_3^-$ and $BO_2^-$unit | [25] |
| ~1620 – 1640 | ------- | P-O-H bond | [24], [26] |
| ~1700 | ($\nu_{as}$) | B-O-B in $BO_3$ triangles | [21] |

($\delta_s$) *Bending,* ($\nu_s$) *Symmetric stretching and* ($\nu_{as}$) *Asymmetric stretching mode of vibration.*

The broadened bands (extended peaks) are observed in the wavenumber ranges between 800 $cm^{-1}$ – 1200 $cm^{-1}$ and 1300 $cm^{-1}$ – 1500 $cm^{-1}$, which arise due to the existence of $B_2O_3$ and $P_2O_5$ polyhedra. Therefore, IR spectrum in the range of 800 $cm^{-1}$ – 1200 $cm^{-1}$ has been deconvoluted for all the glass samples. Fig. 6.4(a-e) illustrates the deconvolution spectra for this range. In the spectra, several peaks are observed at specific wavenumbers, indicating the presence of different vibrational modes and molecular groups within the samples.

One prominent peak appears at 924 $cm^{-1}$, which is attributed to the asymmetric vibration of the $PO_4^{3-}$ group [24], [26], [27]. This peak becomes more pronounced with the addition of $AgI$, indicating an increase in the concentration of the $PO_4^{3-}$ group. However, it is worth noting that this peak is not observed in the sample containing 7 $wt.\%$ of $AgI$. This absence suggests that the concentration of the ($PO_4^{3-}$) group may be lower in this particular sample.

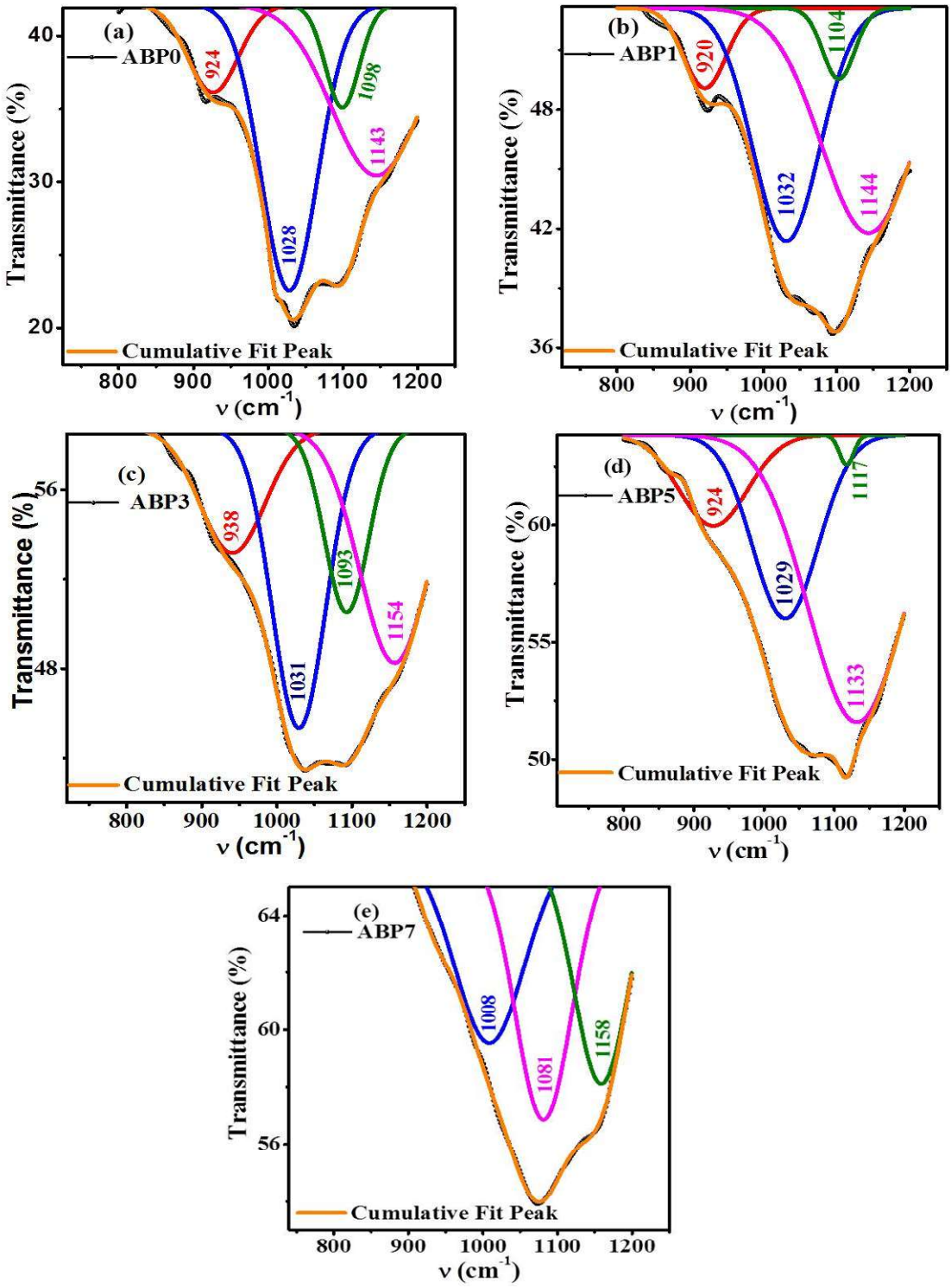


***Figure 6.4**:(a-e) Deconvoluted FTIR spectra in the wavenumber range from 800 $cm^{-1}$ to 1200 $cm^{-1}$ for ABP0 to ABP7 samples.*

Another set of peaks is observed at around 1030 $cm^{-1}$ and at 1098 $cm^{-1}$, which correspond to the asymmetric vibrations of the $BO_4$ and $PO_4$ units units, respectively. These peaks indicate the presence of these molecular groups in the glass samples.

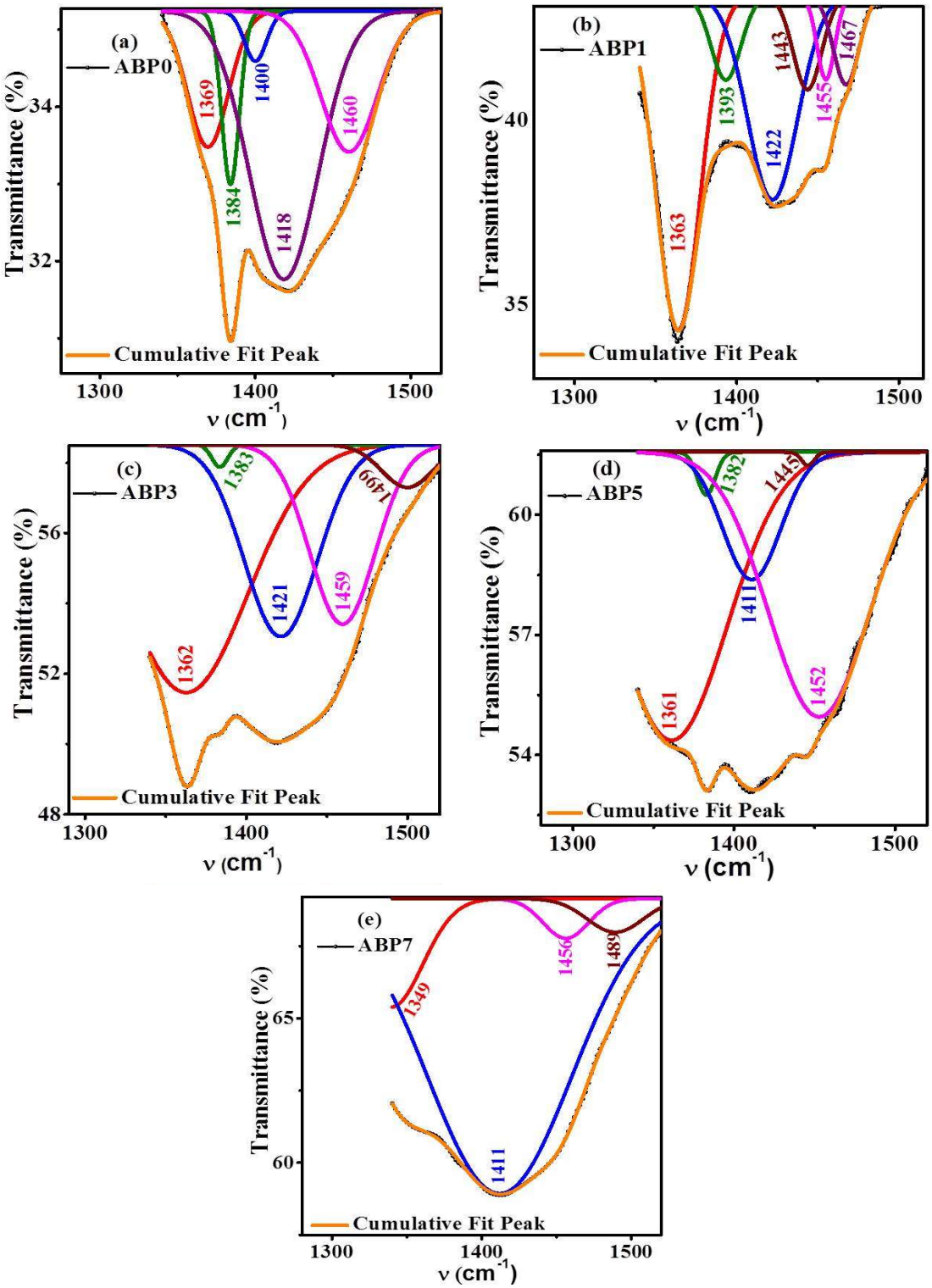


***Figure 6.5**:(a-e) Deconvoluted FTIR spectra in the wavenumber range from 1300 $cm^{-1}$ to 1500 $cm^{-1}$ for ABP0 to ABP7 samples.*

Additionally, the intensity of the peak at 1143 $cm^{-1}$, associated with the $BO_3$ group, is seen to increase with the addition of silver salt [25], [28]. This suggests that the concentration of the $BO_3$ group is influenced by the amount of silver salt added to the samples.

Furthermore, the IR spectrum deconvolution reveals the presence of four absorption bands in the range of 1300 $cm^{-1}$ to 1500 $cm^{-1}$in Fig.6.5(a-e). These bands may be associated with specific molecular vibrations or functional groups present in the glass samples. However, further analysis and characterization would be required to determine the exact nature of these bands and their corresponding molecular species. Based on the IR information, the FTIR spectra analysis suggests the following changes upon the addition of $AgI$:

1. Symmetric Stretching of Pyro and Ortho Borate Groups:
   - Peak at around 1369 $cm^{-1}$: This peak corresponds to the symmetric stretching of the pyro and ortho borate groups in the $BO_3$ molecule [14].
   - Abrupt switch to 1339 $cm^{-1}$ at 7 $wt.\%$ of $AgI$: The addition of $AgI$ causes a shift in the peak position from 1369 $cm^{-1}$ to 1339 $cm^{-1}$, indicating a change in the symmetric stretching behavior of the borate groups.
2. Asymmetric Vibration of Borate Triangle Unit:
   - Peak at 1411 $cm^{-1}$: This peak corresponds to the asymmetric vibration of the borate triangle unit [25].
   - Increase in peak intensity: The presence of $AgI$ leads to an increase in the intensity of this peak, indicating a change in the vibrational behavior of the borate triangle unit.
3. Asymmetric Stretching Bands of $BO_3^-$ *and* $BO_2^-$ Units:
   - Peaks at around 1460 $cm^{-1}$: These peaks correspond to the asymmetric stretching bands of $BO_3^-$ *and* $BO_2^-$ units [25].
   - No change observed: The addition of $AgI$ does not cause any noticeable change in the position or intensity of these peaks, indicating that the asymmetric stretching behavior of these units remains unchanged.

Based on the FTIR spectra analysis, the addition of $AgI$ in the system leads to the following observations:

- Increase in $B-O$ bond length of $BO_4$ and $BO_3^-$ units.
- Formation of asymmetric $PO_4^{3-}$molecules.
- Formation of $P-O-B$ like bridging units.

These changes suggest structural modifications and interactions occurring between the borate and $AgI$ species in the system, leading to alterations in the vibrational behavior of the molecular units.

### 6.3.4 Electrical Characterization / Impedance Spectroscopy

Complex impedance spectroscopy (CIS) of ABP glass series electrolyte samples has been analyzed using impedance formalism technique. The effect of increasing amounts of $AgI$ on the impedance response of the host glass system, $Ag_2O - B_2O_3 - P_2O_5$, is illustrated. The impedance plots for all ABP series compositions over the temperature range of 303 $K$ to 373 $K$, the complex impedance spectra of glasses were measured using the Solartron-1260A for the frequency range of 1 $Hz\ to$ 32 $MHz$.

#### a) DC conductivity

The Nyquist plot in Fig. 6.6(a-f) shows the impedance characteristics of the silver borophosphate glass electrolyte at different temperatures and compositions. The presence of a depressed semi-circle in the Nyquist plot indicates that the sample consists of a combination of resistive $(R)$, capacitive $(C)$, and Warburg $(W)$ elements, suggesting an inhomogeneous distribution within the system. To analyze the experimental results obtained for the silver borophosphate glass electrolyte infused with 5 $wt.\%$ of $AgI$, an equivalent circuit, as illustrated in Fig. 6.7(a), is used. The high-frequency region of the Nyquist plot exhibits a semi-circular feature, which indicates a kinetic-controlled charge transfer mechanism. On the other hand, a spike in the low-frequency region is attributed to the formation of the double layer $(C_{dl})$ at the interface between the electrolyte and electrode, resulting from charge accumulation [31].

Fig. 6.6(f) demonstrates that the intercept $(Z')$ on the real axis of the Nyquist plot exhibits a decreasing trend as the concentration of $AgI$ increases. This intercept value can be used to determine the bulk resistance $(R_b)$ and bulk conductivity $(\sigma_{dc})$ of the glassy electrolyte. To determine the bulk resistance $(R_b)$ and bulk conductivity $(\sigma_{dc})$, one can use the relationships given in Eq. (6.1):

1. Bulk Resistance $(R_b)$: $R_b = (Z')/A$; where $(Z')$ is the intercept on the real axis and $A$ is the area of the electrode/electrolyte interface [32].
2. Bulk Conductivity $(\sigma_{dc})$: $\sigma_{dc} = t/R_b A$ …..(6.1)

Where, $t$ is the thickness of the sample. By analyzing the Nyquist plot and using the intercept $(Z')$ on the real axis, one can calculate the bulk resistance $(R_b)$ and subsequently determine the bulk conductivity $(\sigma_{dc})$ of the silver borophosphate glass electrolyte.

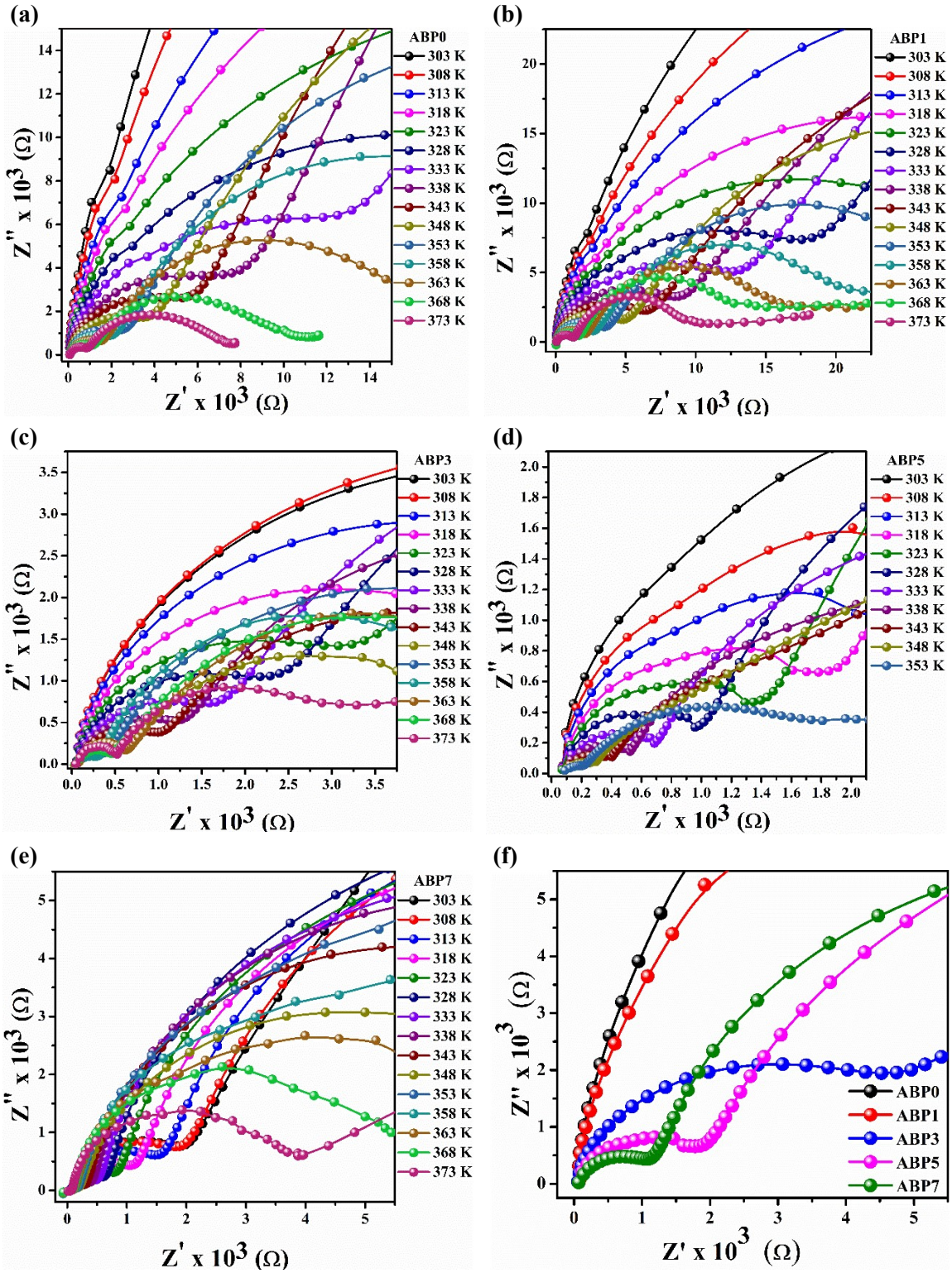


**Figure 6.6**: *Nyquist plots,(a-e) of all glassy electrolytes at various temperatures and (f) for all the samples at* 318 *K temperature.*

Table 6.3 demonstrates that the bulk conductivity of the glassy electrolyte system comprising $AgI - Ag_2O - B_2O_3 - P_2O_5$ exhibits an increase upon the inclusion of $AgI$ up to a concentration of 5 $wt.\%$, followed by a decrease at 7 $wt.\%$ $of$ $AgI$ in the glass.

The temperature-dependent ionic conductivity in disordered systems is typically modelled using two ion transport models: (i) The Arrhenius behavior, and (ii) the nonlinear behavior [33]. Eq. (6.2) demonstrates that the conduction mechanism of ion hopping exhibits Arrhenius behavior.

$$\sigma_{dc} = \sigma_0 Exp(-E_\sigma/K_B T) \quad \ldots (6.2)$$

where, $\sigma_0$ is the conductivity prefactor and appears to be quite insensitive to the composition [31]. Fig. 6.7(b) illustrates the linear representation of the plot of the logarithm of $\sigma_{dc}$ against the reciprocal of temperature $(1000/T)$. The determination of the activation energy $E_\sigma$ was based on the slope of the plots [33]. The activation energy for ABP0 is reported as $0.84\ eV$. Upon the introduction of $AgI$, this value decreases to $0.49\ eV$ till ABP5 sample. However, for the $7\ wt.\%\ AgI$ doped sample, the activation energy increases to $0.52\ eV$, as presented in Table 6.3.

In the present system, $AgI - Ag_2O - B_2O_3 - P_2O_5$ glassy electrolyte, the conductivity $(\sigma_{dc})$ at a temperature of $323\ K$ and the activation energy $(E_a)$ were investigated. The results, as shown in Fig. 6.7(c), indicate that the conductivity increases while the activation energy decreases with the addition of $AgI$ up to a concentration of $5\ wt.\%$. $AgI$ is a compound composed of silver $(Ag)$ and iodine $(I)$, both of which have specific properties. Silver is considered a soft base, while iodine is a soft acid. In the $AgI$ compound, the silver readily dissociates into $Ag^+$ ions and iodine into $I^-$ ions. Many researchers conducted an investigation using Fourier Transform Infrared Spectroscopy (FTIR) to analyse the structural properties of the glassy electrolyte system. They found that the silver ions $(Ag^+)$ from $AgI$ act as modifiers in the system. The presence of $Ag^+$ ions promotes the formation of non-bridging oxygen groups within the structural network of the glassy electrolyte. The increase in non-bridging oxygen groups is observed up to a concentration of $5\ wt.\%\ AgI$. The phenomenon of reduced activation energy and increased conductivity can be comprehended from the perspective of the Anderson-Stuart (A-S) model of ion conduction in glasses, as reported in literatures [34]–[38].

The Anderson-Stuart theoretical framework provides a way to understand ion conduction in terms of activation energy components. According to this framework, the total activation energy $(E_\sigma)$ required for an ion to move can be broken down into two main components: $E_b$ and $E_s$. $E_b$ represents the binding energy, which is the average energy required for a cation to leave its designated site.

***Table 6.3:*** *Activation energy($E_\sigma$), dc conductivity($\sigma_{dc}$), decoupling index ($R_\tau$), carrier concentration ($K'$), hopping frequency ($\omega_p$), relaxation time ($\tau_c$), stretching component ($\beta$) of the AgI doped silver borophosphate glass system.*

| Sample Code | Activation energy $E_\sigma$ $(eV)$ | Calculated at 303 K | | | | | |
|---|---|---|---|---|---|---|---|
| | | Conductivity $\sigma_{dc}$ $x10^{-7}(S\,cm^{-1})$ | Decoupling index $R_\tau$ $x10^7$ | Hopping frequency $\omega_p$ $x10^5$ $(Hz)$ | Carrier concentration K' $x10^{-11}(\Omega^{-1}cm^{-1}Hz^{-1}\,K)$ | Relaxation time $\tau_c$ $x10^{-8}$(second) | Stretching parameter $(\beta)$ |
| ***ABP0*** | 0.84 | 2.42 | 4.84 | 4.75 | 1.09 | 211 | 0.452 |
| ***ABP1*** | 0.69 | 5.86 | 11.7 | 6.01 | 3.28 | 166 | 0.453 |
| ***ABP3*** | 0.56 | 71.9 | 144 | 59.5 | 13.9 | 16.8 | 0.564 |
| ***ABP5*** | 0.49 | 624 | 1250 | 306 | 115 | 3.27 | 0.728 |
| ***ABP7*** | 0.52 | 412 | 824 | 132 | 61.7 | 7.56 | 0.796 |

In other words, it quantifies the energy barrier that needs to be overcome for an ion to detach from its original position and become mobile. $E_s$, on the other hand, corresponds to the elastic strain energy. This component takes into account the energy required to overcome various interactions in the $AgI - Ag_2O - B_2O_3 - P_2O_5$ glassy electrolyte system, these interactions include the electrostatic interactions between $Ag^+$ ions, nearby oxygen species, and iodide ions. $E_s$ can be thought of as the mean kinetic energy that a cation needs to create a "doorway" or a temporary opening in the structure of the glass, allowing it to move through the network of ions and species.

This process involves overcoming the electrostatic forces holding the ions in their respective positions. According to Ghosh et al.; [29], the borophosphate glass skeleton contains different types of borate and phosphate sites that facilitate the hopping of positive alkali ions. When $AgI$ is introduced into the glass framework, it creates desirable anionic sites, including $PO_4^{3-}$, $PO^{2-}$, and $BO_4^{3-}$. The presence of these sites allows the $Ag^+$ ions to be confined within a low-energy potential well. This confinement of $Ag^+$ ions to a low-energy potential well reduces the activation energy required for their movement. As a result, the conductive channels for the motion of mobile cations, such as $Ag^+$ ions, are enhanced. This enhancement leads to an increase in conductivity up to a concentration of 5 $wt.\%$ of $AgI$.

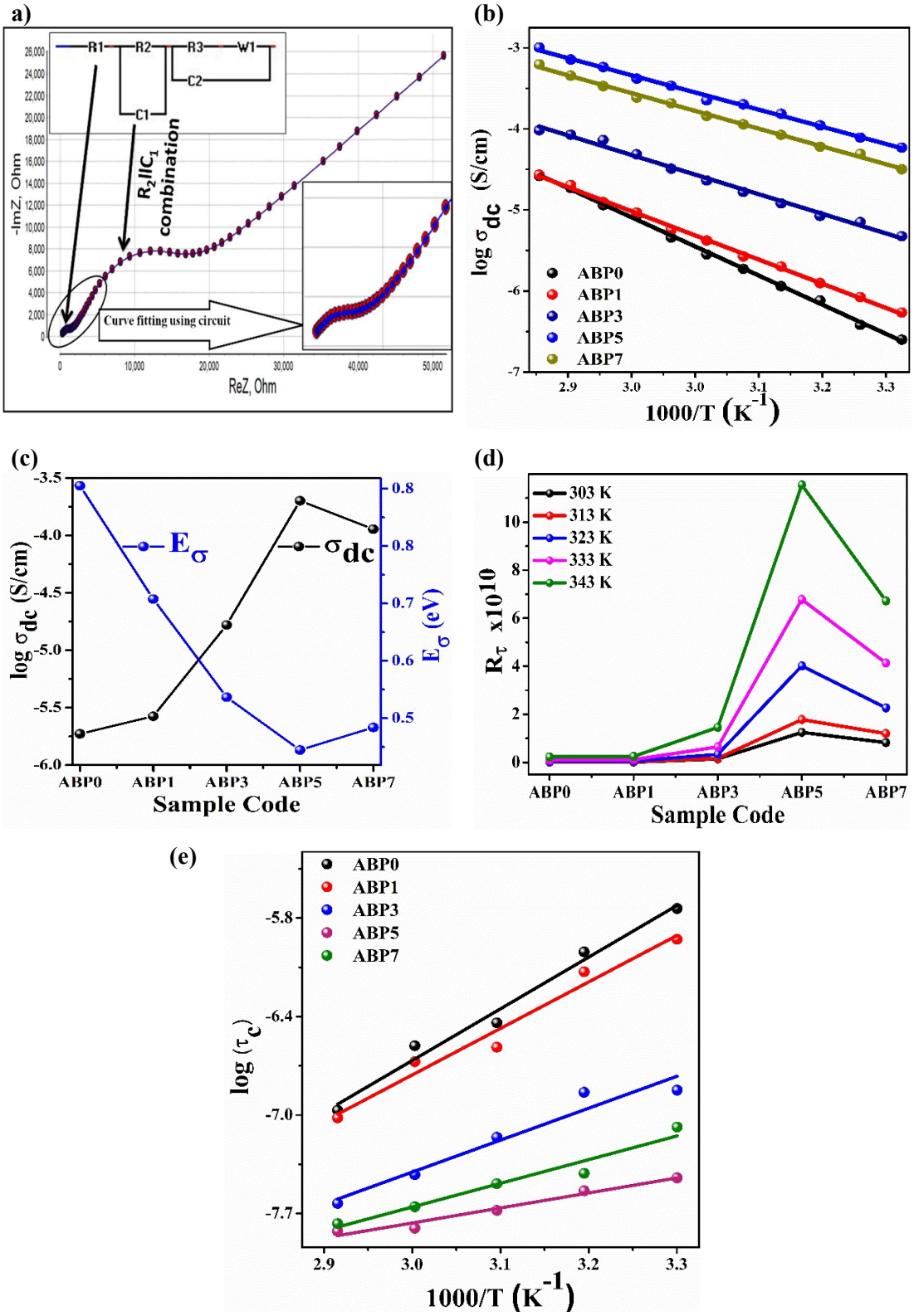


***Figure 6.7**: (a) Nyquist plot fitting and its equivalent circuit for ABP5 for 318 K temperature, (b) the Arrhenius behavior of log $\sigma_{dc}$ conductivity vs reciprocal of temperature plot, (c) variation of dc conductivity and the activation energy as a function of AgI content, (d) plot of concentration of decoupled silver ions as a function of glass composition, (e) plot of the conductivity relaxation time vs reciprocal of temperature.*

Furthermore, the introduction of $Ag^+$ ions causes a transition in their local coordination environment. Initially, the coordination environment is predominantly oxygen-exclusive. However, with the addition of $AgI$, the coordination environment shifts to a completely iodide ($I^-$) environment. This transition in the local coordination environment can result in a reduction in conductivity or an increase in the activation energy ($E_\sigma$) required for ion hopping. Overall, the incorporation of $AgI$ into the borophosphate glassy electrolyte system modifies the anionic sites, confines $Ag^+$ ions to low-energy potential wells, and alters their local coordination environment. These changes contribute to the observed increase in conductivity up to a certain concentration of $AgI$, while higher concentrations may result in a reduction in conductivity or an increase in activation energy. In the study, the relationship between conductivity and composition is further supported by the decoupling index $R_\tau$, as shown in Fig. 6.7(d). The decoupling index ($R_\tau$) is a measure used in ionically conducting glass systems to quantify the degree to which mobile ions are decoupled from the glass matrix [18]. The decoupling index is defined as the ratio of the average structural relaxation time ($\tau_s$) to the mean conductivity relaxation time ($\tau_c$) at the glass transition temperature ($T_g$). The structural relaxation time ($\tau_s$) represents the time it takes for the glassy structure to undergo structural rearrangements, while the conductivity relaxation time ($\tau_c$) represents the time scale for ionic motion contributing to conductivity. In the study, the value of $\tau_s$ at $T_g$ is reported to be 200 seconds [39]. On the other hand, the values of $\tau_c$ at $T_g$ are determined by extrapolating the $\log \tau_c$ versus $1000/T$ graph to the glass transition temperature ($T_g$), as illustrated in Fig. 6.7(e). By comparing the values of $\tau_s$ and $\tau_c$, the decoupling index ($R_\tau$) provides insights into the extent to which the mobile ions are decoupled from the glass matrix. A higher decoupling index indicates a greater degree of decoupling, suggesting that the mobile ions can move more freely within the glassy structure. The plotted decoupling index ($R_\tau$) in Fig. 6.7(d) confirms the relationship between conductivity and composition. As the conductivity increases with the addition of $AgI$ up to a certain concentration, it is expected that the decoupling index ($R_\tau$) will also show a corresponding increase, indicating a higher degree of decoupling between mobile ions and the glass matrix.

As indicated in Table 6.3, that $R_\tau$ values show a consistent increase as the $AgI$ content in the glass composition increases. This suggests that the presence of $AgI$ has an effect on the measured parameter, resulting in higher values. The upward trend in $R_\tau$ values continues until a specific threshold of 5 wt.% of $AgI$ is reached. Beyond this point, the relationship

may change or plateau, indicating a potential limit or saturation in the influence of $AgI$ on the parameter being measured. The decoupling index is a measure of the degree to which $Ag^+$ ions, become detached or separated from the glass matrix. An increase in the decoupling index indicates a decrease in the viscosity of the glass network structure. The decrease in glass viscosity due to the addition of $AgI$ promotes the migration or movement of $Ag^+$ ions within the glass structure. The increased decoupling index suggests that $Ag^+$ ions are becoming more liberated or detached from the glass matrix. As the decoupling index increases in correlation with the $AgI$ content, it allows for more efficient transport of $Ag^+$ ions.

### b) Frequency dependent conductivity

Fig. 6.8(a-e) displays the frequency-dependent behaviour of ac conductivity ($\sigma'$) for various concentrations of $AgI$ in ABP glass compositions at various temperatures. Meanwhile, Fig. 6.8(f) illustrates the frequency-dependent behaviour of ac conductivity for all the samples at $323\ K$ temperature. Typically, three crossover regions can be observed in the system under consideration. First crossover region is located in the lower frequency range and is attributed to polarization effects occurring at the electrodes. When an electric field is applied, the polarization of the material at the electrode interfaces can affect the conductivity measurements. This region may show deviations or changes in the conductivity behavior due to electrode polarization phenomena. Second crossover region is observed in the mid frequency range and exhibits a frequency independent plateau. This means that within this frequency range, the conductivity remains relatively constant regardless of the applied frequency. The plateau indicates a frequency-independent behavior and suggests that certain processes or mechanisms are dominant within this frequency range, Fig. 6.8(e). Third crossover region is located in the high frequency range and is characterized by a rapid increase in conductivity with frequency. In this region, the conductivity of the system significantly increases as the frequency of the applied electric field increases. This behavior indicates the presence of specific conduction mechanisms or processes that become more significant at higher frequencies [32], [40]. Additionally, the statement mentions the extrapolation of the region of the plateau, characterized by a zero value of $\sigma(\omega)$, for the purpose of determining the value of $\sigma_{dc}$ . This extrapolation involves extending the frequency-independent region to determine the value of dc conductivity ($\sigma_{dc}$ ) at zero frequency.

The data pertaining to the conductivity that varies with frequency was subjected to analysis utilising Jonscher's universal power law.

$$\sigma'(\omega) = \sigma_{ac}=(\sigma_{dc} + A\omega^{n}) \quad \ldots (6.3)$$

where, symbol $A$ represents a constant value, while $\omega$ denotes the radial frequency, and $n$ represents the frequency dependent power exponent factor.

It was stated that the conductivity frequency response observed in glasses can be explained by the translational and localized hopping of ions. These mechanisms are responsible for the electrical transport in glasses at different frequency ranges as stated in the previous study [39]. Translational hopping refers to the movement of ions over long distances, allowing for electrical transport at low frequencies. This means that at low frequencies, the ions in the glass can move and contribute to the conductivity over relatively large distances. This mechanism is associated with the long-range diffusion of ions, enabling electrical conduction to occur.

On the other hand, high frequency dispersion in glass conductivity can be attributed to the forward-backward hopping of ions. In this case, the ions move in a more localized manner, requiring less energy compared to the long-range diffusion observed at low frequencies. The forward-backward hopping mechanism allows the ions to move within a limited region, without traveling long distances. This localized hopping contributes to the conductivity response at high frequencies.

The hopping frequency, denoted as $\omega_p$, represents the frequency at which the relaxation effects become noticeable. At frequencies below $\omega_p$, the translational hopping mechanism dominates, and electrical transport occurs over long distances. At frequencies above $\omega_p$, the forward-backward hopping mechanism becomes more significant, leading to high frequency dispersion in the conductivity response. It has been observed that the value of $\omega_p$ increases with temperature, as indicated by the shift towards the higher frequency side, as depicted in Fig. 6.8(f). The calculation of $\omega_p$ can be performed using Eq. 6.4, and the corresponding values are presented in Table 6.3.

$$\omega_p=\left((\sigma_{dc}/A)^{1/n}\right) \ldots (6.4)$$

where, $\omega_p$ is assumed to be present at $\sigma_{ac} = 2\sigma_{dc}$ (Fig. 6.8(f)) for all samples at $323\ K$ temperature.

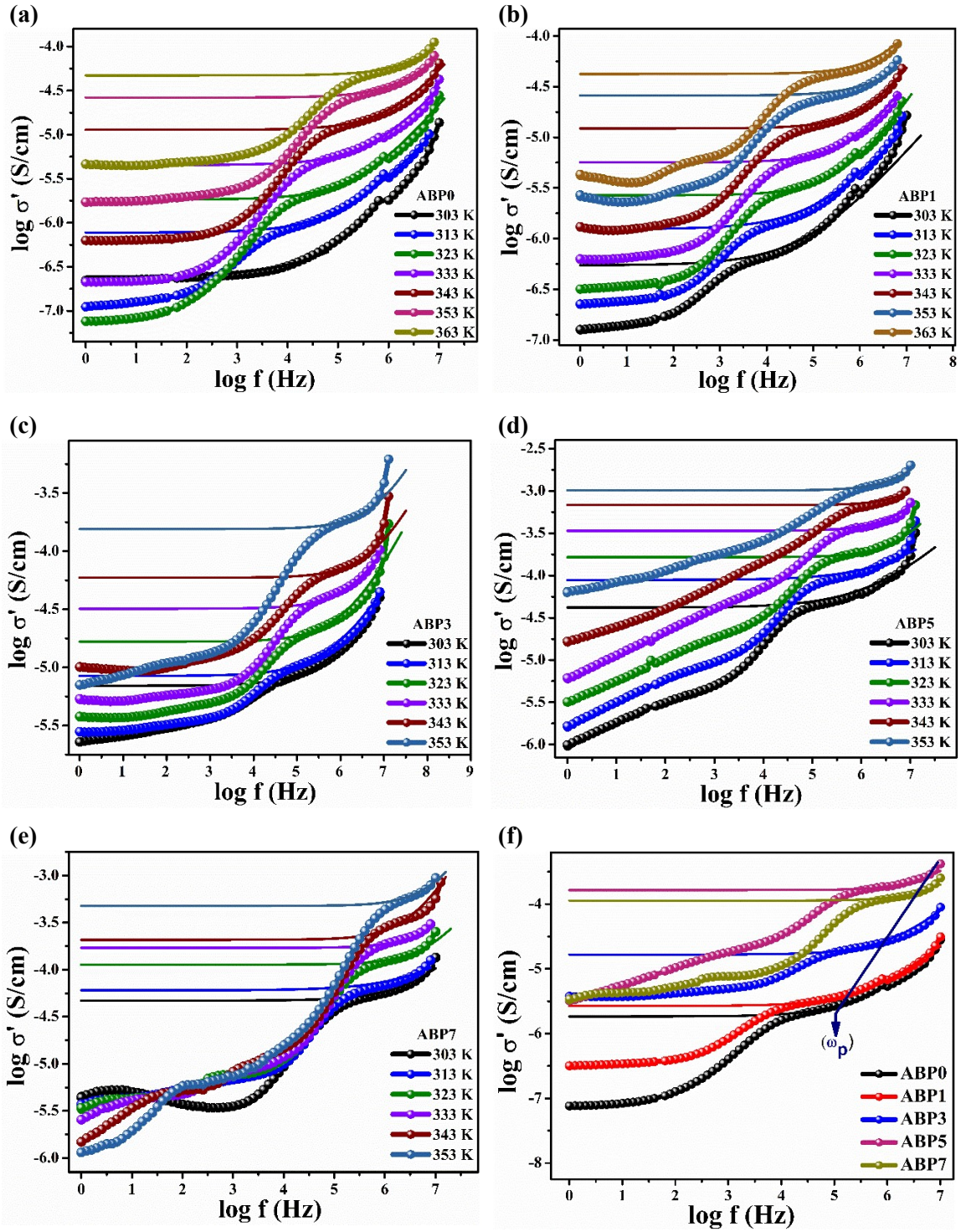


***Figure 6.8**: (a-e) The plots of σ′ vs frequency at various temperatures for $x = 0, 1, 3, 5$ and 7 wt.% of AgI in the borophosphate glass respectively, (f) at 323 K temperature, JPL fitting for all the samples exhibiting the hopping frequency (straight line represents the JPL fitting and guide to eyes).*

### Ion transport model

Fig. 6.9(a) illustrates the relationship between the power law exponent ($n$) and temperature for various glass compositions. The exponent ($n$) in the range of 0.51 to 0.73 has been observed in studies examining the conductivity frequency response in glasses. This exponent is used to characterize the level of interaction between mobile ions and the host framework.

In the context of the Non-Overlapping Small Polaron Tunneling Model (NSPT) [41], [42], the value of the exponent ($n$) has been found to exhibit an increase in correlation with temperature. This means that as temperature increases, the value of ($n$) tends to increase as well, indicating a stronger interaction between the mobile ions and the glass framework. According to the findings of M. Dult et al; [42], a decrease in the value of the exponent ($n$) suggests a higher degree of interaction between the ions and the glass framework. This higher degree of interaction can lead to modifications in the network structure of the glass. Fig. 6.9 (a) illustrates that the ABP5 sample exhibits the lowest value of ($n$) across all temperatures, indicating a significant level of interaction between the mobile ions and the framework. The inset of Fig. 6.9 (a) describes the variation of the power exponent factor as a function of temperature for ABP5 sample. In the lower frequency region, a sharp decrease in the derivative of conductivity with respect to frequency ($\sigma'(\omega)$) is observed in glasses. This phenomenon is attributed to the accumulation of a higher number of charges at the electrode-electrolyte polarization interface. In other words, at lower frequencies, there is a build-up of charges near the electrode-electrolyte interface, leading to a decrease in the conductivity derivative. In the intermediate frequency range, specifically at frequencies lower than the peak frequency ($\omega < \omega_p$), the conductivity exhibits a nearly constant behavior with respect to frequency. This means that within this frequency range, the conductivity does not show significant changes as the frequency varies. The observed nearly constant behavior of conductivity in this frequency range can be explained by the higher velocity of ions in the glass. The higher ion velocity enables them to transit between unoccupied sites more readily, resulting in a relatively stable conductivity response. This finding is consistent with the results reported by S. Murugavel et al; in their study [43].

In the present glass systems, the direct current conductivity ($\sigma_{dc}$) results from the successful hopping of an ion to an adjacent vacant site. When the frequency surpasses the hopping frequency ($\omega > \omega_p$), the ionic conductivity starts to increase as the frequency rises.

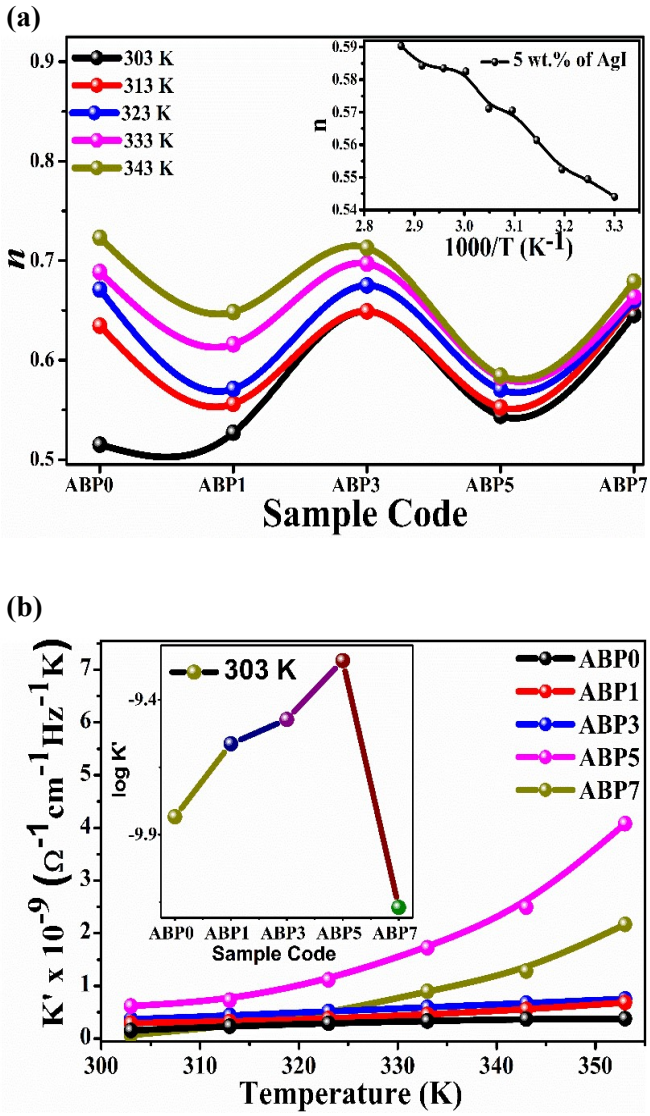


The phenomenon of conductivity relaxation occurs due to the transition from a frequency-independent conductivity to dispersive conductivity. The jump relaxation model [44], [45] can explain the observed frequency dependence of conductivity in these glass systems.

According to the theoretical framework of the jump relaxation model, at low frequencies, the mobile ion has sufficient time intervals to effectively migrate to an adjacent unoccupied site. This migration contributes to the direct current conductivity ($\sigma_{dc}$), leading to the appearance of a plateau region in the conductivity response.

**Figure 6.9:** *(a) frequency power exponent* ($n$) *as a function of glass composition at various temperatures-inset: for ABP5 sample the temperature dependent variation of power exponent, (b) variation of mobile ion concentration* ($K'$) *as a function of temperature for all glass compositions-inset:* $K'$ *for all the compositions at room temperature.*

After an ion completes its initial movement from one site to a neighboring site, two relaxation processes can be observed. The first process involves the ion returning to its initial position, which is known as correlated forward-backward hopping. The second process involves the relaxation and shifting of the neighboring cage potential of ion cloud with respect to its new position. These relaxation processes and the associated changes in the ion positions contribute to the dispersive conductivity behavior observed at frequencies higher than the hopping frequency ($\omega > \omega_p$). At higher frequencies, the time intervals available for the ion to return to its original location become reduced. This leads to an increased probability of the ion undergoing correlated forward-backward hopping, where it

returns to its initial position after hopping to a neighboring site. The increased probability of this process, along with the relaxation of the cage potential of the neighboring ion cloud, contributes to the observed high frequency conductivity dispersion in alternating current (ac) conductivity spectra.

The mobile ion concentration factor, denoted as $K'$ [46], plays a significant role in influencing conductivity. This factor represents the concentration of mobile ions in the material. The mobile ion concentration factor, $K'$, can influence conductivity through its impact on various processes, such as ion hopping and relaxation of the cage potential. A higher concentration of mobile ions increases the likelihood of ion hopping events and correlated forward-backward hopping, thereby affecting conductivity. The calculation is derived from Eq. 6.5, and the corresponding numerical values are presented in Table 6.3.

$$K' = \frac{\sigma_{dc} T}{\omega_P} \quad \ldots (6.5)$$

The variation of $K'$ that is as a function of temperature for the glass samples, is shown in Fig. 6.9(b). It is observed that the $K'$ increases slightly up to ABP3 with changing temperature, while a larger increase is observed for ABP5 and ABP7 samples. The inset of Fig. 6.9(b) describes that the charge carrier concentration factor varies almost linearly with increasing $AgI$ up to $5\,wt.\%$ and then decreases for ABP7 glass sample at room temperature.

- **Conductivity scaling**

The scaling laws, such as the Summerfield scaling [47], Roling scaling [48], and Ghosh scaling [49], are mathematical equations used to describe the conductivity behavior of semiconducting materials in relation to various parameters. These scaling laws allow for the prediction and analysis of conductivity based on existing quantities and scaling parameters. In the Summerfield canonical scaling, the ratio of the complex conductivity $(\sigma')$ to the dc conductivity $(\sigma_{dc})$ is expressed as a function of frequency $(f)$, the dc conductivity at a given temperature $(\sigma_{dc})$, the absolute temperature $(T)$, and the dopant concentration $(x)$. The equation suggests that the conductivity ratio depends on the frequency, temperature, and dopant concentration.

$$\frac{\sigma'}{\sigma_{dc}} = F\left(\frac{f}{\sigma_{dc} T}\, x\right) \ldots\ldots \quad (Summerfield\ canonical\ scaling)$$

where, $f$ is the frequency, $\sigma_0 = \sigma_{dc}$ is the conductivity at a given temperature, $T$ is the absolute temperature, $x$ is dopant concentration. At $\omega = \omega_p$, $\sigma'(\omega) = 2\sigma_{dc}$.

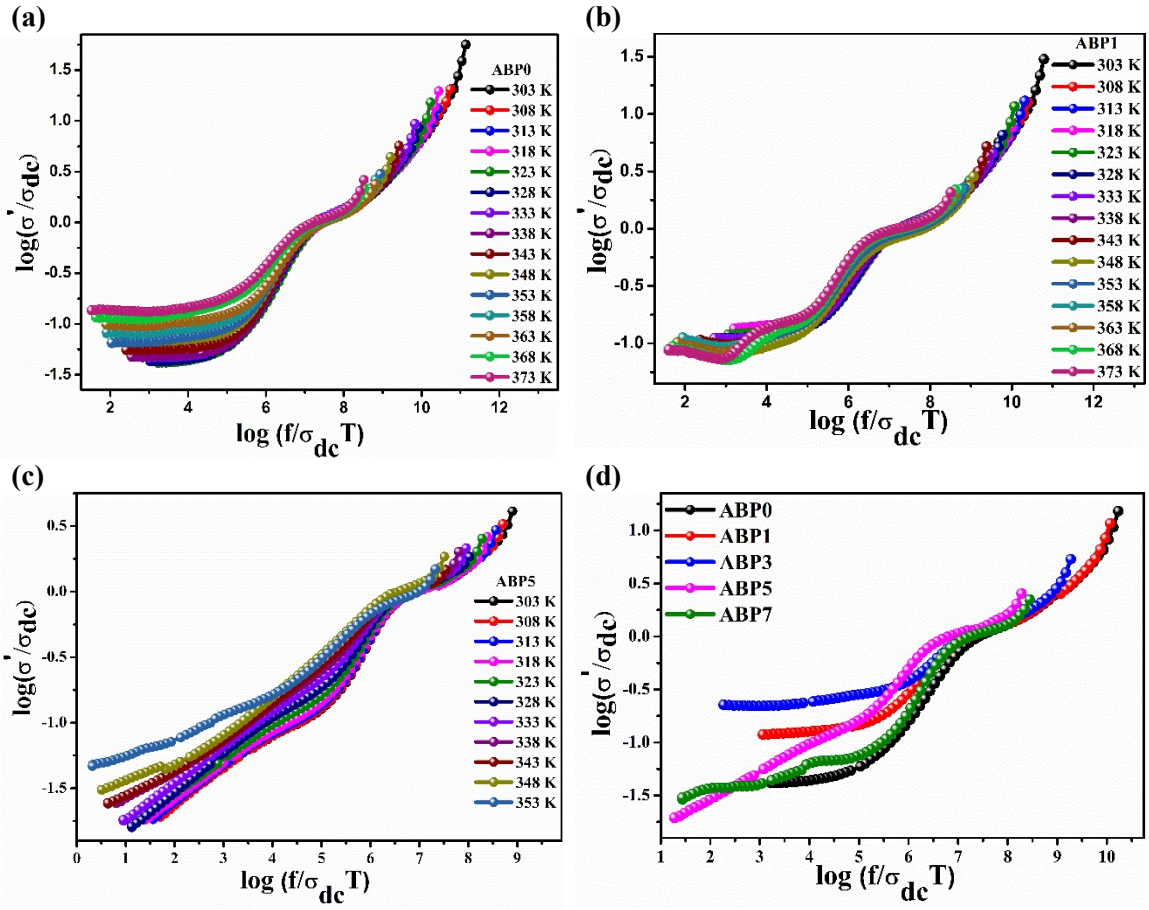


***Figure 6.10**: Plots of scaled conductivity spectra with frequency using Roling formulation (a-c) at different temperatures, (d) at 323 K for all the glass samples.*

The Roling canonical scaling assumes that charge carriers are independent of temperature, and the frequency ($\omega_p$) is a thermally activated factor with the same energy as $\sigma_{dc}T$. In this scaling law, the ratio of $\sigma'$ to $\sigma_{dc}$ is expressed as a function of frequency ($f$) and the dc conductivity at a given temperature ($\sigma_{dc}$). The Ghosh scaling also considers the ratio of σ' to $\sigma_{dc}$, but it expresses it as a function of frequency ($f$) and the plasma frequency ($f_p$).

$$\frac{\sigma'}{\sigma_{dc}} = F\left(\frac{f}{\sigma_{dc}T}\right) \quad \ldots\ldots (Roling\ canonical\ scaling)$$

$$\frac{\sigma'}{\sigma_{dc}} = F\left(\frac{f}{f_p}\right) \quad \ldots\ldots (Ghosh\ canonical\ scaling)$$

The ion dynamics are described by the universal function $F$, which remains unaffected by variations in temperature and chemical composition. The advantage of using these scaling laws is that they provide a way to relate conductivity behavior to existing quantities, such as frequency, dc conductivity, temperature, and dopant concentration. This allows for the characterization and prediction of conductivity based on known parameters, making it a valuable tool in the study of semiconducting materials.

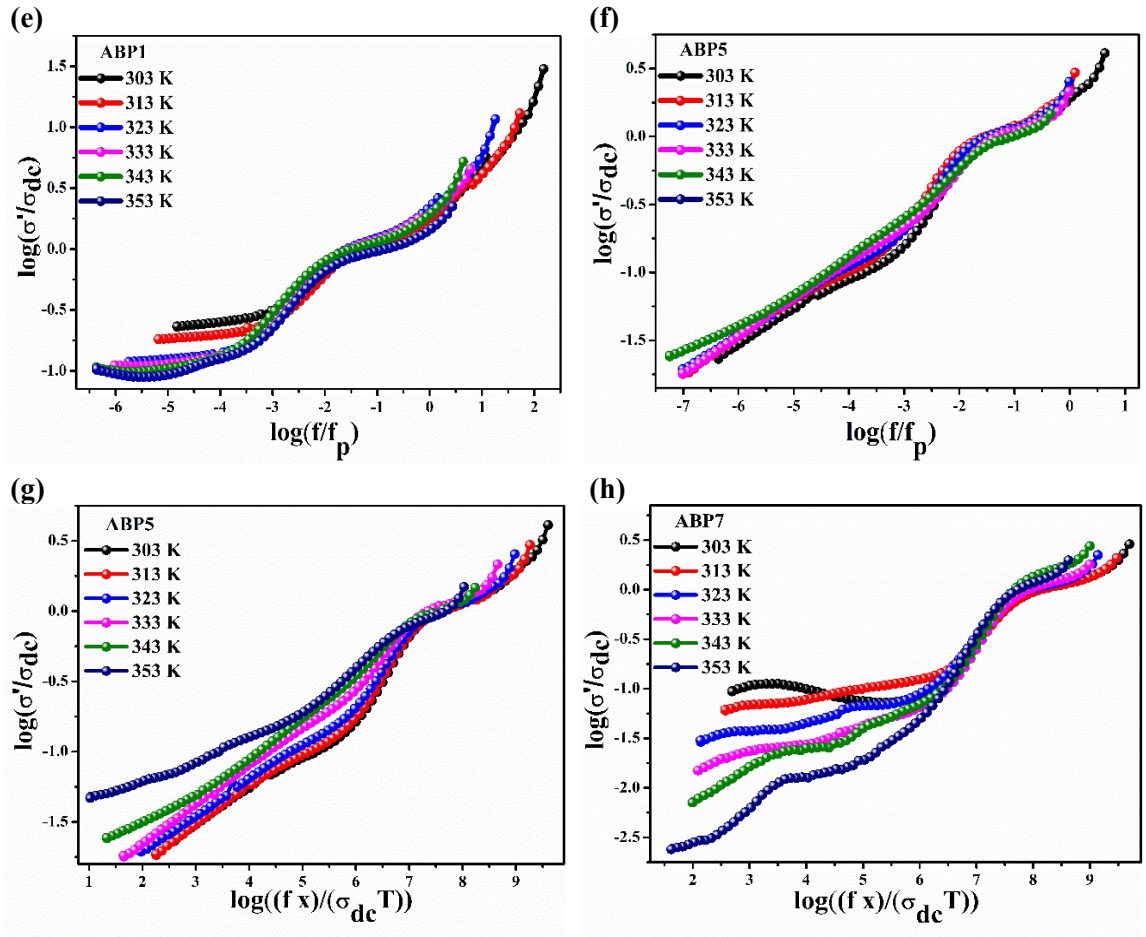


***Figure 6.10**: Plots of normalized conductivity spectra with frequency using (e-f) Ghosh model of scaling, and (g-h) Summerfield formalism.*

In Fig. 6.10 (a-d), the data presented demonstrates the scaling of ac conductivity ($\sigma'(\omega)$) with respect to dc conductivity ($\sigma_{dc}$) using different formalisms, such as the Roling [48], Ghosh [49] (Fig. 6.10(e-f)), and Summerfield [47] (Fig. 6.10(g-h)) formalisms, to normalize the frequency axis for all the glasses at various temperatures.

According to Sidebottom [53], the scaling method used in this context is referred to as canonical scaling. Canonical scaling preserves the shape of the ac conductivity spectrum as temperature changes, while maintaining the invariance of the ion concentration.

The near-perfect merging of all conductivity spectra at various temperatures into a single master curve suggests both a time-temperature superposition (TTS) and a temperature-independent conduction mechanism. This merging indicates that the conductivity response can be scaled and shifted along the frequency axis to align with the temperature. The scaled conductivity spectra of each glass composition at 323 $K$ are shown in Fig. 6.10(d), and they converge into a single curve. This convergence demonstrates the composition

independence of ionic conductivity, indicating that the nature of ion transport is not strongly influenced by the specific composition of the glass.

However, it is noted that at very low frequencies, particularly close to the polarization region, none of the spectra merge completely. This discrepancy might be attributed to a change in the concentration of mobile $Ag^+$ ions or a slightly different ion transport behavior in the glass at that specific temperature. It suggests that at extremely low frequencies, there may be factors that affect the conductivity response and prevent a complete merging of the spectra.

According to Dyre et al; [50], the TTS phenomenon is observed in single-ion conducting glasses and crystals with structural disorder. It arises due to the disorder in the glass matrix, which leads to a wide range of potential energies for the ions. As a result, there is a variation in the ion site energies and barrier heights [51], [52].

The Rolling formulation is considered the most suitable among other formulations used in the current glass series for conductivity scaling. Conductivity scaling refers to a method used to analyze the behavior of conductivity in different conditions. In this case, the scaling method employed suggests that conductivity relaxation in the glass series is independent of time, temperature, and composition, except at low frequencies where it depends on the concentration of mobile ions [48].

### c) Dielectric Study

The dielectric relaxation spectra provide information about the dynamic and relaxation characteristics of the electric dipoles present in a system. It helps to understand how these dipoles respond to an alternating electric field and how they relax back to their original state after each cycle. The real part of permittivity, denoted as $\varepsilon'$, is similar to the conventional dielectric constant of a material. It represents the quantification of electric potential energy stored within a specific volume of the material under the influence of an alternating electric field. This energy is released back into the field at the end of each cycle and is observed as induced polarization [54]. The dielectric loss factor, represented by $\varepsilon''$, indicates the degree of energy absorption by the material. When subjected to an alternating electric field, a fraction of electrical energy is converted into heat. The application of an external electrical field leads to charge transfer, increasing the energy losses experienced by the dielectric material. The dielectric loss tangent, denoted as $\tan\delta$, is a parameter that quantifies the dielectric losses. It is calculated as the ratio of the dielectric loss factor ($\varepsilon''$) to the real part

of permittivity ($\varepsilon'$). It provides information about the efficiency of energy conversion from electrical to heat energy in the material. In summary, it highlights the concepts of dielectric relaxation, permittivity, dielectric loss factor, and the calculation of dielectric losses using the dielectric loss tangent.

**Complex Permittivity:**

The complex permittivity, denoted as $\varepsilon^* = \varepsilon' - i\varepsilon''$, is a useful tool for understanding the frequency dependence of dielectric absorption. It consists of a real part ($\varepsilon'$) and an imaginary part ($\varepsilon''$), which represent the storage and dissipation of electrical energy, respectively. The behavior of dielectric losses is influenced by specific characteristics of the physical mechanisms governing the dispersion of electrical energy in a dielectric material. Both frequency and temperature play a role in this dependence. At frequencies below $10^3\ Hz$, there are mechanisms that cause a delay in the migration of polarization. These mechanisms impact the dielectric losses and contribute to the frequency dependence observed in this range. Within the frequency range of $10^3 - 10^8\ Hz$, there is a delay in thermally activated polarization. This mechanism also affects dielectric losses and contributes to the frequency dependence observed in this range.

The retardation of polarization, caused by the aforementioned mechanisms, leads to a decrease in the value of $\varepsilon'(\omega)$ as the frequency increases. This reduction is associated with the peak observed in the loss factor $\varepsilon''(\omega)$. In summary, the passage highlights the importance of the complex permittivity for characterizing dielectric absorption and its frequency dependence. It also discusses the specific mechanisms, such as the delay of migration mechanisms of polarization and thermally activated polarization, that contribute to the frequency and temperature dependence of dielectric losses. However, without the specific reference provided as [54], it is not possible to provide further context or details from that particular study.

Fig. 6.11 (a-e) represents variation of dielectric constant $\log \varepsilon'(\omega)$ with $\log f$ for the present series samples. Upon analyzing the data pertaining to dielectric properties, it is evident that the dielectric constant $\varepsilon'(\omega)$ exhibits a negative correlation with frequency, ultimately reaching a saturation point at higher frequencies by converging towards the limiting value of $\varepsilon(\infty)$. This phenomenon can be attributed to the occurrence of rapid polarization within the glass material [55]. The disappearance of the capacitive effect at sites with high free energy barriers is observed at higher frequencies, leading to a decrease in the dielectric

constant. These findings are consistent with the observations reported by previous researchers [56]–[60]. All the samples exhibit analogous characteristics in their dielectric dispersion spectra.

Increasing the temperature leads to a shift of the frequency dispersion towards higher frequencies in the dielectric constant. This means that the behavior of the dielectric constant changes with temperature, with a greater impact on higher frequency ranges.
In the case of silver-borophosphate glass, the observed frequency dispersion can be attributed to several factors:

a. This refers to the polarization occurring at the interfaces between different phases or regions within the material. It can arise due to variations in composition, structure, or other properties at the interfaces.
b. This is due to the lack of uniformity or variation in the structure of the material. Variations in the arrangement of atoms or ions can cause differences in the dielectric response at different frequencies.
c. Space charges can form within the material due to the presence of mobile charges or defects. These charges contribute to the dielectric behavior and can result in frequency dispersion.

In order to understand dielectric relaxation in vitreous ionic conductors accurately, it is important to subtract the contribution of direct current (dc) conductivity ($\sigma_{dc}/\omega\varepsilon_0$) from the complex dielectric permittivity ($\varepsilon^*$). This is because the presence of mobile charges in the material can suppress dielectric relaxation peaks. The remaining portion of the complex permittivity ($\varepsilon^*$) after subtracting the dc conductivity contribution can be expressed as:

$$\varepsilon^* = \varepsilon' - j\varepsilon''_{corrected} = \varepsilon' - j\left[\varepsilon'' - \frac{\sigma_{dc}}{\omega\varepsilon_0}\right] \quad \ldots\ldots (6.6)$$

Here, $\varepsilon'$ represents the real part of the permittivity, $\varepsilon''$ represents the imaginary (loss) part of the permittivity, $\varepsilon''_{corrected}$ represents the dielectric loss value for a single frequency relaxation process (such as a Debye model), $\sigma_{dc}$ is the dc conductivity, ω is the angular frequency, and $\varepsilon_0$ is the vacuum permittivity. The experimental findings indicate that the complex permittivity ($\varepsilon^*$) manifests across a wider frequency spectrum. This can be attributed to the distribution of relaxation times, meaning that the relaxation processes occur at different rates or timescales within the material. It is mentioned that the current system lacks polar molecules but still exhibits direct current conductivity.

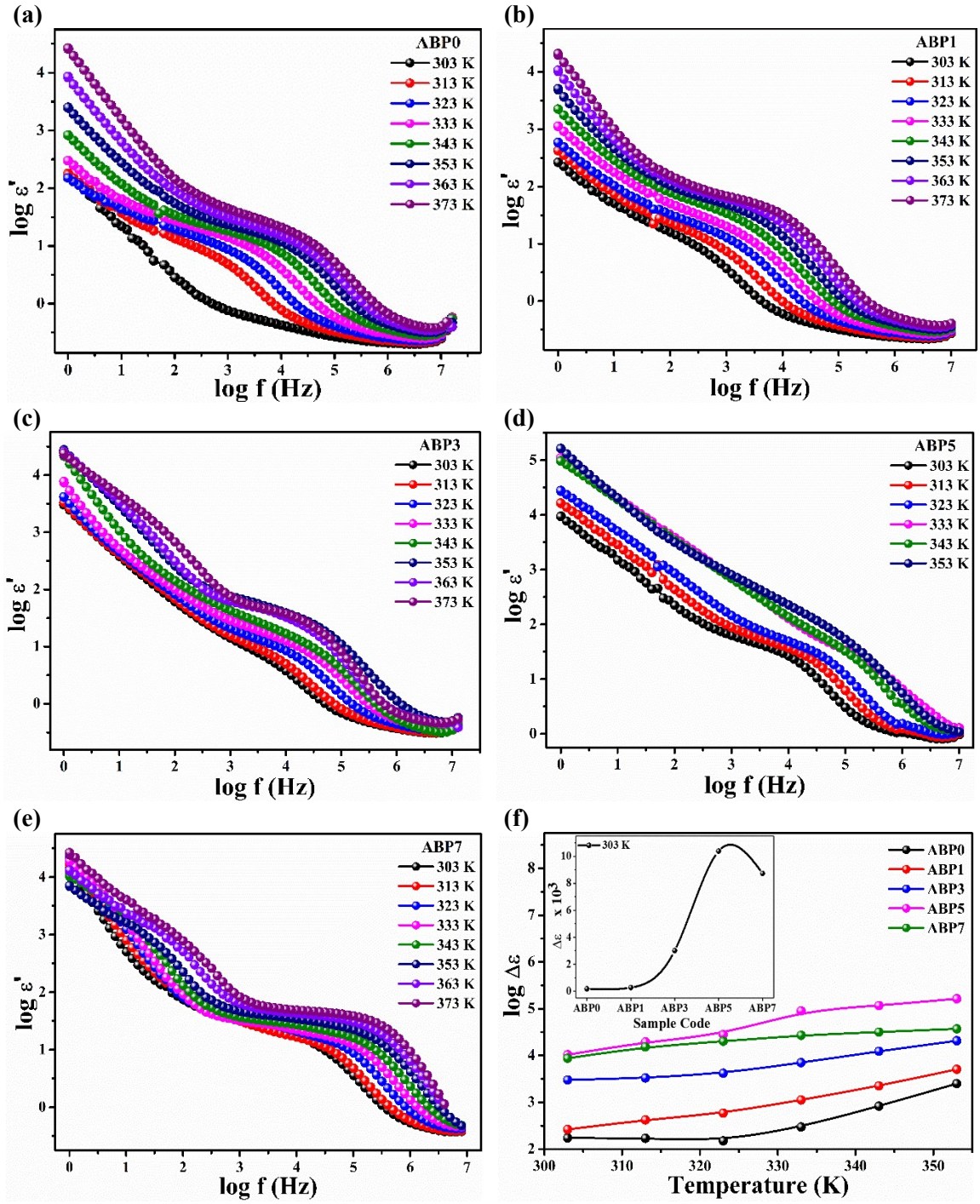


***Figure 6.11**: (a-e) Plots of dielectric constant spectra ($\varepsilon'$) with frequency for all the glass samples, (f) Dielectric strength($\Delta\varepsilon = \varepsilon_s - \varepsilon_\infty$) for all the glass samples at various temperature (inset: at 303 K temperature), the variation of net polarization as a function of glass compositions.*

Dielectric relaxation caused by ionic motion in the material is referred to as "migration losses" [59], [60]. This suggests that the ionic species within the material contribute to the dielectric behavior and relaxation processes.

In ionic crystals, the free energy barriers for ion movement are uniform throughout the lattice. However, in glassy materials, there is variation in the free energy barriers between different sites. The conduction in these materials can be described as ions jumping along lattice sites. At low frequencies, the $Ag^+$ ions migrate from sites with low energy barriers in the direction of the electric field. As they move, they accumulate at sites with high energy barriers. This accumulation leads to a net polarization or dielectric strength ($\Delta\varepsilon = \varepsilon_s - \varepsilon_\infty$) of the ionic medium, which can be obtained from the plot of the real part of the dielectric constant ($\varepsilon'$) as shown in Fig. 6.11(f & inset). The frequency-dependent variation of $\varepsilon'$ in the studied glass systems is attributed to the long-range diffusion of $Ag^+$ ions. This diffusion involves multiple jumps over barriers of different heights. At high frequencies, the electric field reverses its direction rapidly enough that excess ionic jumps in the field direction do not occur. As a result, the polarization caused by the accumulation of charges at high free energy barrier sites disappears. This leads to a decrease in the observed value of $\varepsilon'$ towards $\varepsilon_\infty$, which represents the dielectric constant at very high frequencies. This transition occurs when the frequency ($\omega$) of the applied field is much larger than the inverse of the characteristic jump time ($1/\tau$) out of low-free energy barrier sites.

The dielectric loss spectrum ($\varepsilon''$) of the ABP glass system was analyzed by studying the influence of sodium iodide dopant salt on the imaginary component of permittivity ($\varepsilon''$) as a function of frequency at various temperatures, as depicted in Fig. 6.12(a-e). The variations in $\varepsilon'$ and $\varepsilon''$ indicate the occurrence of the Non-Debye phenomenon. This phenomenon suggests that the frequency-dependent space charge regions arise from ion diffusion and the formation of a space charge region at the electrode-electrolyte interface [61], [62]. As mentioned earlier, the conductivity of the glass samples increases with temperature due to thermal stimulation.

However, no significant loss peak is observed in any of the glass samples across the analysed frequency range. High dielectric loss is typically observed in materials with high ionic conductivity. In this case, the high dielectric constant is primarily attributed to significant ionic conductivity, with electronic conductivity playing a minor role, as mentioned in reference [63].

It's worth noting that the dielectric loss in these materials is approximately 100 times greater than the dielectric constant. This indicates that the dissipation of energy in the material due to the dielectric loss is much higher than the energy storage capacity represented by the dielectric constant.

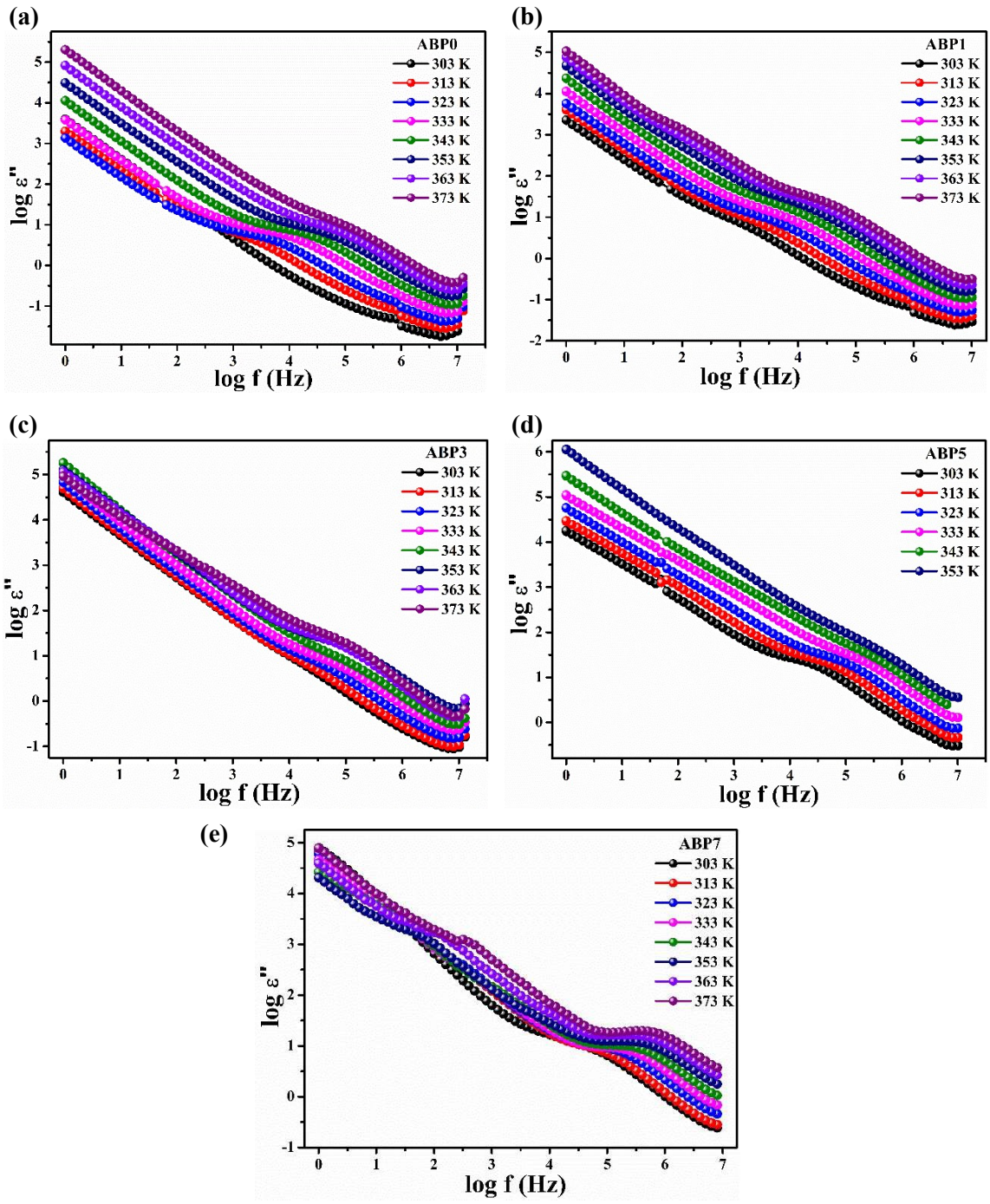


***Figure 6.12:****(a-e) Plots of dielectric loss* ($\varepsilon$"*) spectra with frequency at different temperature for various glass compositions.*

Fig. 6.13(a-e) shows the frequency-dependent behavior of $\log[\varepsilon^{"} - (\sigma_{dc}/\omega\varepsilon_0)]$ for samples with different concentrations of silver iodide salt, $AgI$ $(x = 0, 1, 3, 5, 7\ wt.\%)$, at various temperatures. Fig. 6.13(f) displays $\log[\varepsilon^{"} - (\sigma_{dc}/\omega\varepsilon_0)]$ as a function of $log\ f$ for all the samples at a temperature of $323\ K$. The plots indicate an inverse relationship between $\varepsilon^{"}$and frequency $(1/\omega)$, as well as a decrease in $\varepsilon^{"}$ with increasing temperature.

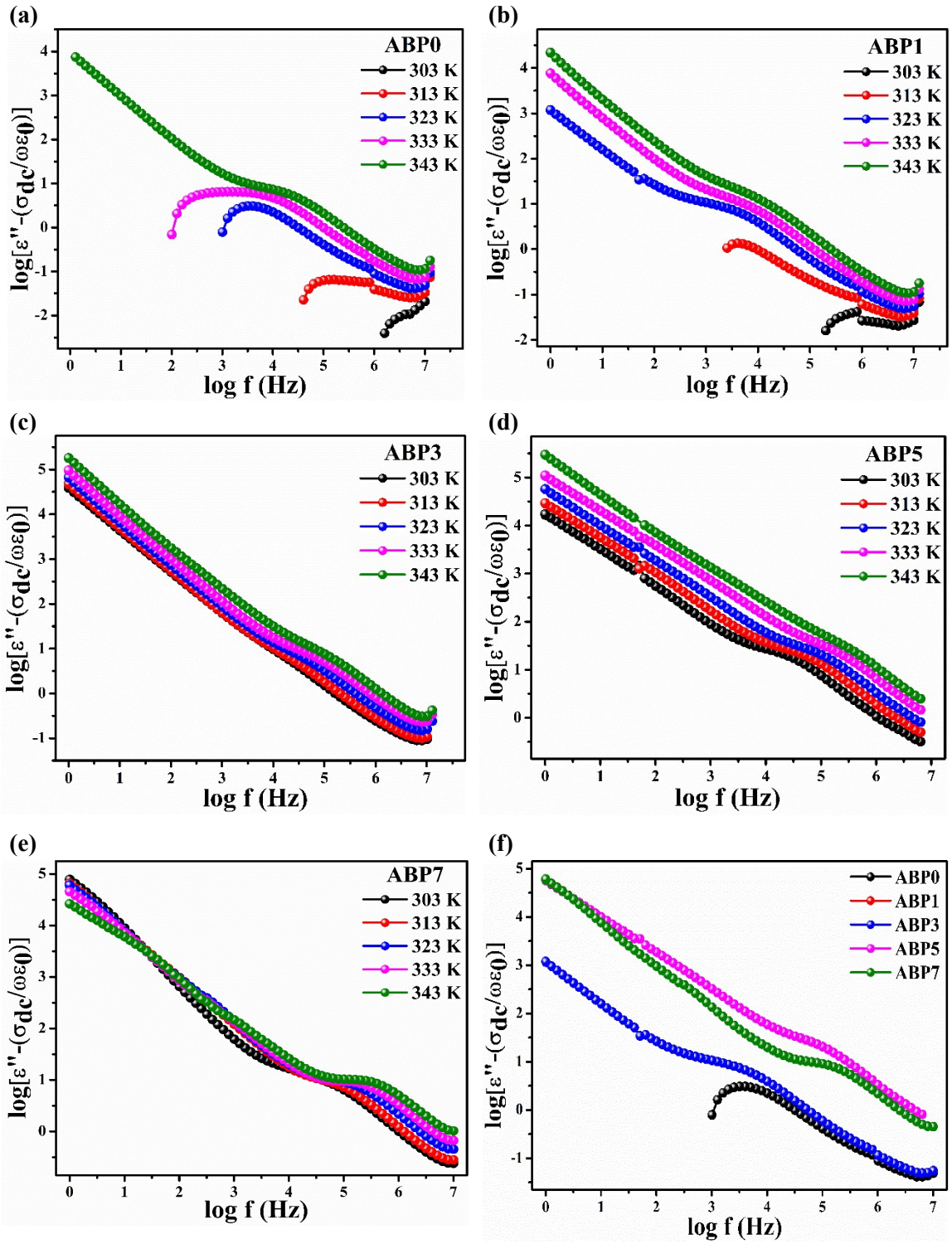


***Figure 6.13:*** *Plot of* $log[\varepsilon^{"} - (\sigma_{dc}/\omega\varepsilon_0)]$ *with log f for all the glass compositions.(a-e) at various temperatures, and (f) at 323 K temperature.*

Similar observations have been reported by researchers worldwide [56], [58], [64] for other glasses that conduct $Ag^+$ ions. The dielectric relaxation loss in the radio frequency range is a combination of dipole relaxation and conduction, and these combined losses are often referred to as migration losses.

The magnitude of conduction losses is influenced by the direct current conductivity, denoted as $\sigma_{dc}$, which can be calculated using formula (6.7):

$$\varepsilon''_{\sigma_{dc}} = \frac{\sigma_{dc}}{\omega\varepsilon_0} \quad \ldots\ldots (6.7)$$

These losses occur due to the effect of an electric force. The mobile ions move through the amorphous structure, dissipating a portion of the energy acquired from the electrical force into the structure as thermal energy. As the temperature increases, the conduction loss also increases due to the corresponding increase in $\sigma_{dc}$ and its shift towards lower frequencies at lower temperatures. The corrected value of dielectric loss ($\varepsilon''_{corrected}$) at different frequencies and temperatures can be calculated using the following expression, based on the known value of dc conductivity ($\sigma_{dc}$). Therefore, it is important to subtract $\sigma_{dc}/\omega\varepsilon_0$ for $x = 0, 1, 3, 5$ and $7\ wt.\%$ from $\varepsilon''$ in order to distinguish between the effects of conduction losses and migration losses. Fig. 6.13 (a-f) show a peak after eliminating the dc contribution, the maximum of which shifts to higher frequencies as the temperature rises. The corrected $\varepsilon''$ value shows a significant reduction in comparison to the $\varepsilon''$value, indicating the clear contribution of dipole relaxation.

Fig. 6.14(a) and (b) show the temperature dependence of the real and imaginary components of dielectric permittivity for a concentration of $5\ wt.\%$ of $AgI$ in the ABP glass system, at different frequencies ranging from $10\ Hz$ to $1\ MHz$. In the frequency range of $10\ Hz$ to $10\ kHz$, both the real ($\varepsilon'$) and the imaginary component ($\varepsilon''$) of the dielectric constant exhibit an increasing trend with rising temperature. This behavior is observed at lower frequencies because as the temperature increases, the mobility of ions within the glass matrix also increases. This enhanced mobility allows the ions to move in parallel with the applied electric field, resulting in an elevation of the permittivity components. However, as the frequency surpasses $10\ kHz$, the magnitudes of $\varepsilon'$ and $\varepsilon''$ exhibit a reduced level of enhancement with increasing temperature. This is because, at higher frequencies, the charge carriers (ions) experience limited mobility in response to the rapidly varying electric field. As a result, the real and imaginary components of permittivity remain relatively stable in the specified temperature range. For $1\ MHz$ frequency range, the comparable patterns of the real ($\varepsilon'$) and imaginary ($\varepsilon''$) components of dielectric permittivity can also be observed in the glass specimen, as shown in Fig. 6.14(c) and (d). At lower frequencies, the mobility of ions, specifically silver ions ($Ag^+$), is facilitated as they can easily escape from sites with low energy barriers in response to the applied electric field.

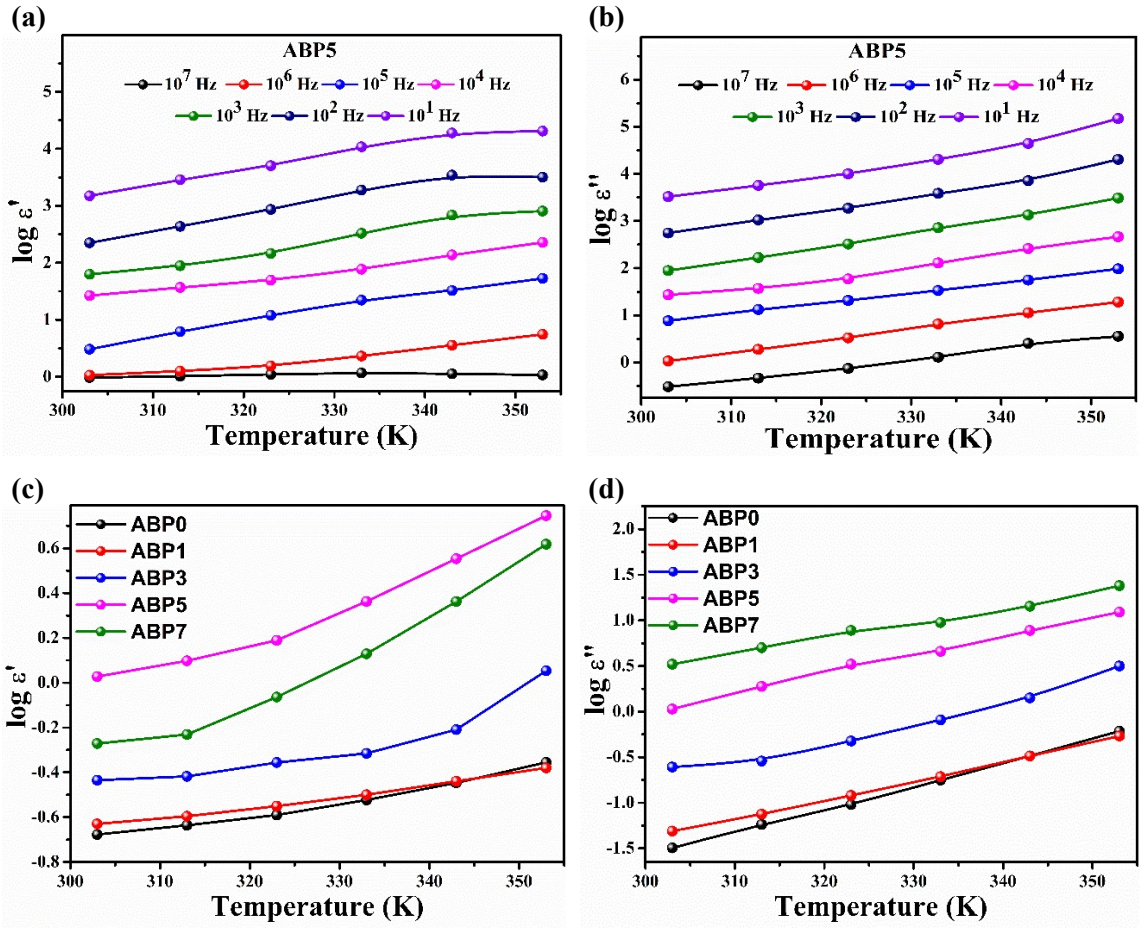


***Figure 6.14**:(a) $\log \varepsilon'$ and (b) $\log \varepsilon''$ for ABP5 sample for various frequency values, (c) and (d) are $\log \varepsilon'$ and $\log \varepsilon''$ respectively for all the glass samples as a function of temperature for the frequency* 1 *MHz.*

However, these ions tend to accumulate at sites with high energy barriers, resulting in the manifestation of a dielectric relaxation strength ($\Delta\varepsilon = \varepsilon_s - \varepsilon_\infty$). This strength represents the net polarization magnitude of the ionic medium, as depicted in Fig. 6.11(f). The phenomenon of dielectric relaxation strength ($\Delta\varepsilon$) is primarily attributed to thermal effects. From Fig. 6.11(f and inset), it is observed to gradually increase with rising temperature.

The polarization that occurs is a result of microscopic phenomena and is influenced by factors such as the concentration of mobile ions and the hopping distance they can traverse. As per Eq. 6.8, the loss tangent-tan $\delta$, also known as the dielectric loss angle, of a system is indicative of the correlation between the energy dissipated per radian in the material and the energy stored at the point of polarization peak.

$$\tan\delta = \frac{\varepsilon''_{(\omega)}}{\varepsilon'_{(\omega)}} \quad \ldots (6.8)$$

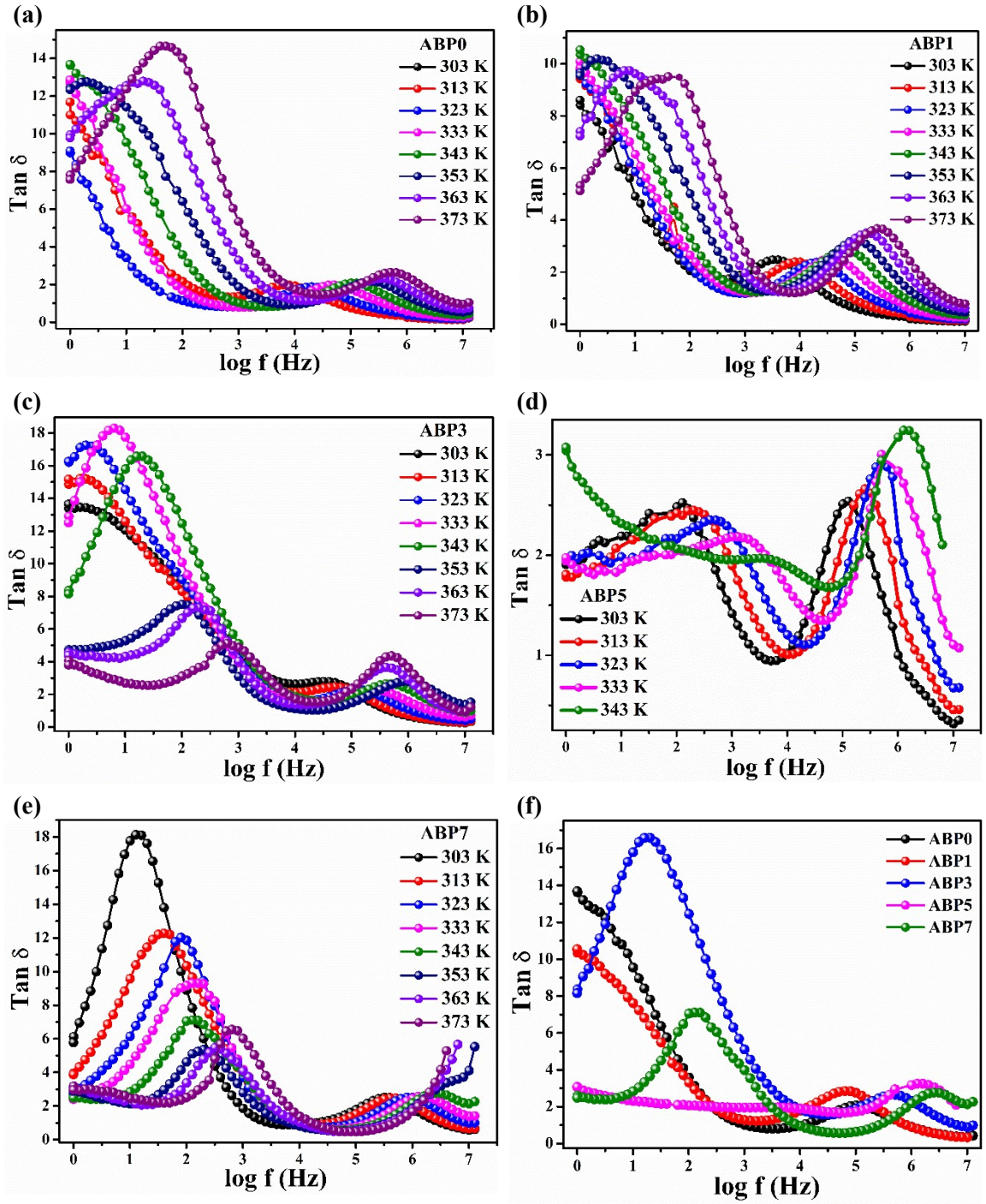


***Figure 6.15**: Plots of tan δ spectra with frequency, (a-e) at different temperature for ABP0, ABP1, ABP3, ABP5 and ABP7 glass compositions, (f) for various glass samples at 343 K.*

Fig. 6.15(a-e) depict the plot of the tangent of the loss angle $(\tan\delta)$ versus the logarithm of frequency $(\log f)$ for all ABP glass compositions at various temperatures. These graphs demonstrate that the tan δ value is more dependent on temperature in the high-frequency regime compared to the low-frequency regime. As the frequency increases, $\tan\delta$ rapidly drops until it appears to flatten at frequencies above 100 $MHz$.

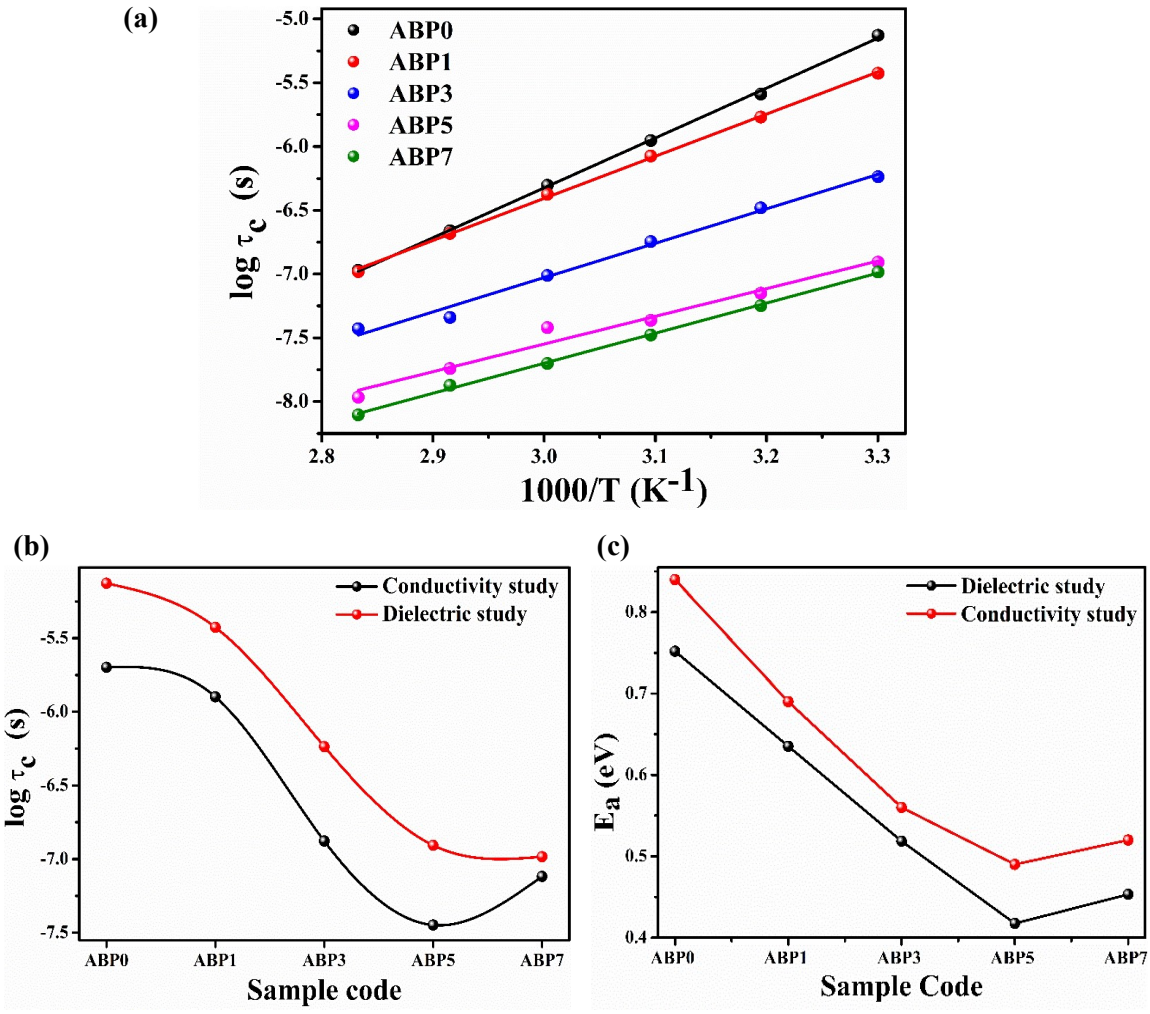


***Figure 6.16:*** *(a) Dielectric Relaxation time ($\tau$) vs inverse of temperature for all the glass compositions, (b) Comparison of conductivity and dielectric relaxation time for ABP glass series, (c) Similarity between the activation energy obtained from dielectric study and conductivity study for various dopant concentrations in the host glass system.*

The $\tan\delta$ plot indicates that the frequency dispersion shifts towards higher frequencies as the temperature rises. This means that the peak in the loss angle occurs at higher frequencies at higher temperatures. This behavior is observed across different compositions of the ABP glass system. Fig. 6.15(f) shows the relationship between $\tan\delta$ and $log\ f$ for different dopant concentrations at a temperature of $343\ K$. The loss peak $(\tan\delta)$ is at a minimum for the ABP5 sample, which is also evident from Fig. 6.15(d). As depicted in the graph, the dispersion region shifts to higher frequencies as the dopant concentration increases. Additionally, the sudden decrease in $\tan\delta$, followed by a consistent value at higher frequencies, indicates an inverse proportionality between $\tan\delta$ and a certain power of frequency. The graphical representation in Fig. 6.16(a) illustrates the correlation between the dielectric relaxation time and the reciprocal of temperature for various concentrations of AgI, while Fig. 6.16(b) displays the correlation between the dielectric relaxation time

and conductivity relaxation time with the glass compositions and finds the similar trend. The activation energy $E_a$ derived from the relaxation plot ($\tau$) is comparable to that obtained from the corresponding conductivity plots ($\sigma$), Fig. 6.16(c), indicating that the flow of charge carriers determines the relaxation time. The motion of mobile charge carriers, specifically $Ag^+$ ions, contributes to both- the conductivity and the relaxation effects.

### d) Electric Modulus Study

The analysis of relaxation events in terms of the electrical modulus provides insights into the transition from frequency-independent conductivity to frequency-dependent conductivity, while also accounting for polarization effects at the electrode-electrolyte interface. The modulus formalism, as proposed by Macedo et al. [64], captures relaxation processes driven by ion mobility in superionic glasses. To understand ion relaxation and its behavior with respect to temperature and/or frequency in ionic conducting systems such as glasses or polymers, several models have been proposed by researchers [48], [65]–[71].

According to the findings of Macedo et al. [64], the electrical modulus ($M'$) can be obtained by taking the reciprocal of the complex dielectric permittivity ($\varepsilon'$), and can be represented as follows:

$$M^* = \frac{1}{\varepsilon_0} = M' + iM'' \quad \ldots\ldots (6.9)$$

Here, $M'$ and $M''$ denote the real and imaginary components of the electric modulus, respectively.

The electrical modulus provides a convenient way to analyze the relaxation behavior of ions in ionic conducting systems and is a useful tool for understanding the dynamics of ion motion as a function of temperature and frequency.

Moynihan et al; [71] introduced the Kohlrausch-Williams-Watts (KWW) relaxation function empirically to describe the width of the $M''$ peaks, which are commonly associated with a stretching exponent $\beta$. The equation proposed by them is:

$$\emptyset(t) = e^{\left(-\frac{t}{\tau}\right)^{\beta}} \quad \ldots\ldots (6.10)$$

The stretching parameter $\beta$ is typically found to be between 0 and 1 (Non-Debye) by fitting frequency-dependent plots of the imaginary part of the electric modulus ($M''$).

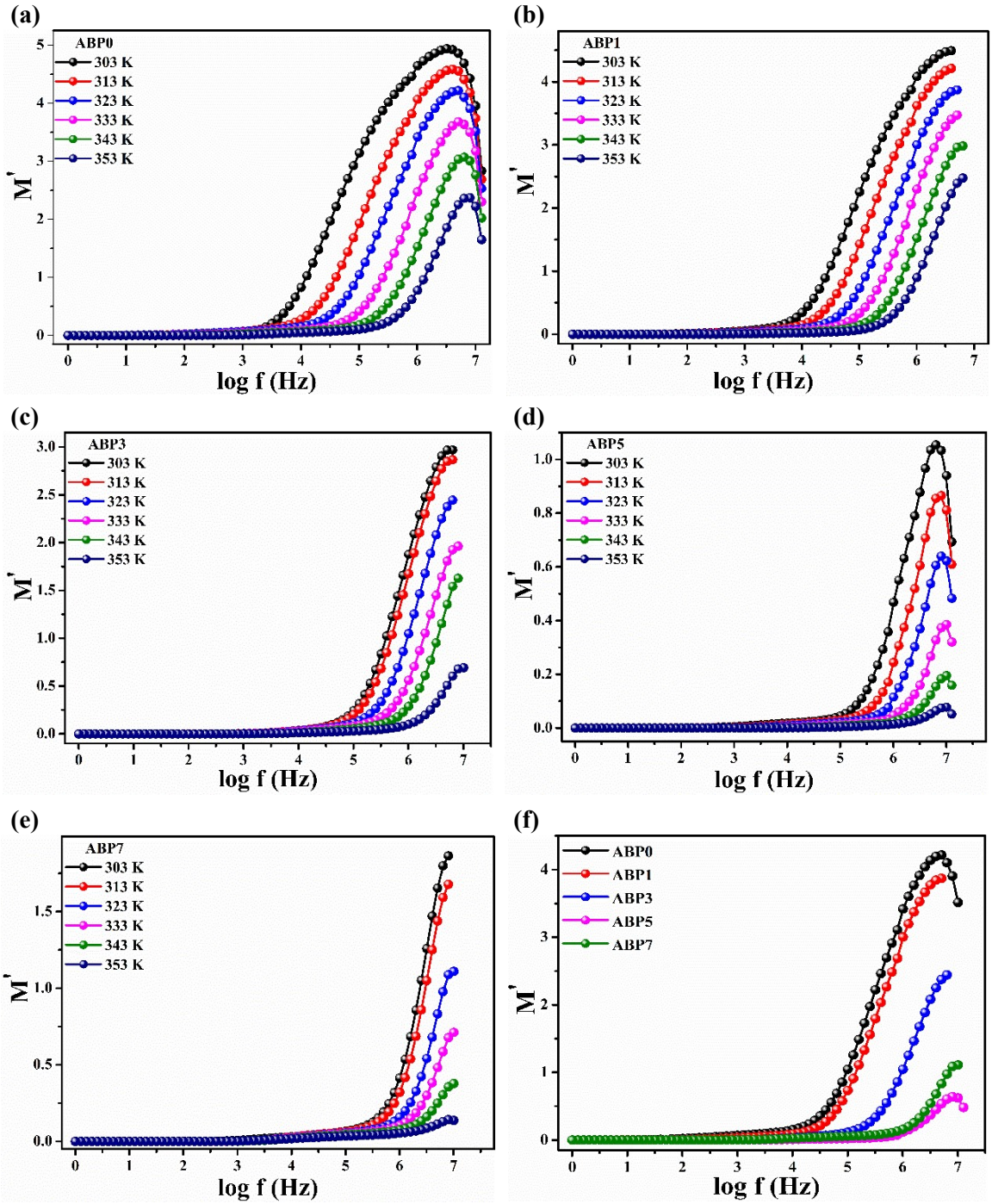


***Figure 6.17:*** *Plots of M' vs. logarithmic function of frequency, (a-e) respectively for ABP0 to ABP7 samples at different temperatures, (f) all the glass samples at 323 K.*

The coupling model, formulated by Ngai and Kannert [72], illustrates the relationship between the power-law dependence of conductivity and the KWW relaxation mechanism. According to this model, Eq. 6.10 can be expressed as:

$$\sigma_{kww} = B\ exp\left(-\frac{E_a}{K_B T}\right)\omega^{1-\beta} \quad \ldots\ldots (6.11)$$

Here, $\sigma_{kww}$ represents the conductivity described by the KWW relaxation mechanism, $B$ is a pre-exponential factor, $E_a$ is the activation energy for the relaxation process, $K_B$ is the Boltzmann constant, $T$ is the temperature, ω is the angular frequency, and $\beta$ is the stretching parameter. The relationship between the activation energy for direct current conduction ($E_\sigma$) and the activation energy ($E_a$) can be established through the stretching parameter $\beta$, as given by:

$$E_a / E_\sigma = \beta \quad \ldots\ldots (6.12)$$

This relationship allows for the connection between the activation energy for relaxation processes and the activation energy for direct current conduction, providing insights into the dynamics of ion motion and conductivity in the material. In this current study, the real part of the modulus ($M'$) demonstrates dispersion, reaching its maximum and shifting towards higher frequencies, as depicted in Fig. 6.17(a-f).

Fig. 6.18(a-f) illustrates the frequency-dependent imaginary part of the modulus ($M$"). The $M$" curve exhibits a prolonged and flat tail, extending from the low frequency range to the intermediate frequency range. This behavior is primarily attributed to the capacitance associated with the electrodes. At higher frequencies, the modulus starts to increase due to the bulk effect and reaches its maximum value or peak. It has been observed that the peak of M" shifts towards higher frequencies with increasing temperature, accompanied by varying peak heights. Regardless of temperature, the $M$" curves exhibit the same shape, differing only in terms of peak position and Full Width at Half Maximum (FWHM) values. The average relaxation time can be determined by the conductivity relaxation frequency $\omega_c$that corresponds to $M''_{max}$, under the condition that $\omega_c\tau_c$=1 [73]. The frequency ranges below $M''_{max}$is associated with long-range mobility of charge carriers, while the frequency range above $M''_{max}$is associated with short-range mobility due to confinement of charge carriers within potential wells. The temperature-dependent shift in $f_{max}$ position is explained by the frequency distribution of barrier cross-over. The $M''$ curves width is linked to the relaxation times distribution, which is associated with the distribution of free energy barriers for ionic jumps. This distribution increases with greater disorder or due to the cooperative nature of the conduction process. The temperature dependence of $M''$ can be attributed to the thermal activation of charge carriers, resulting in increased mobility and decreased relaxation time.

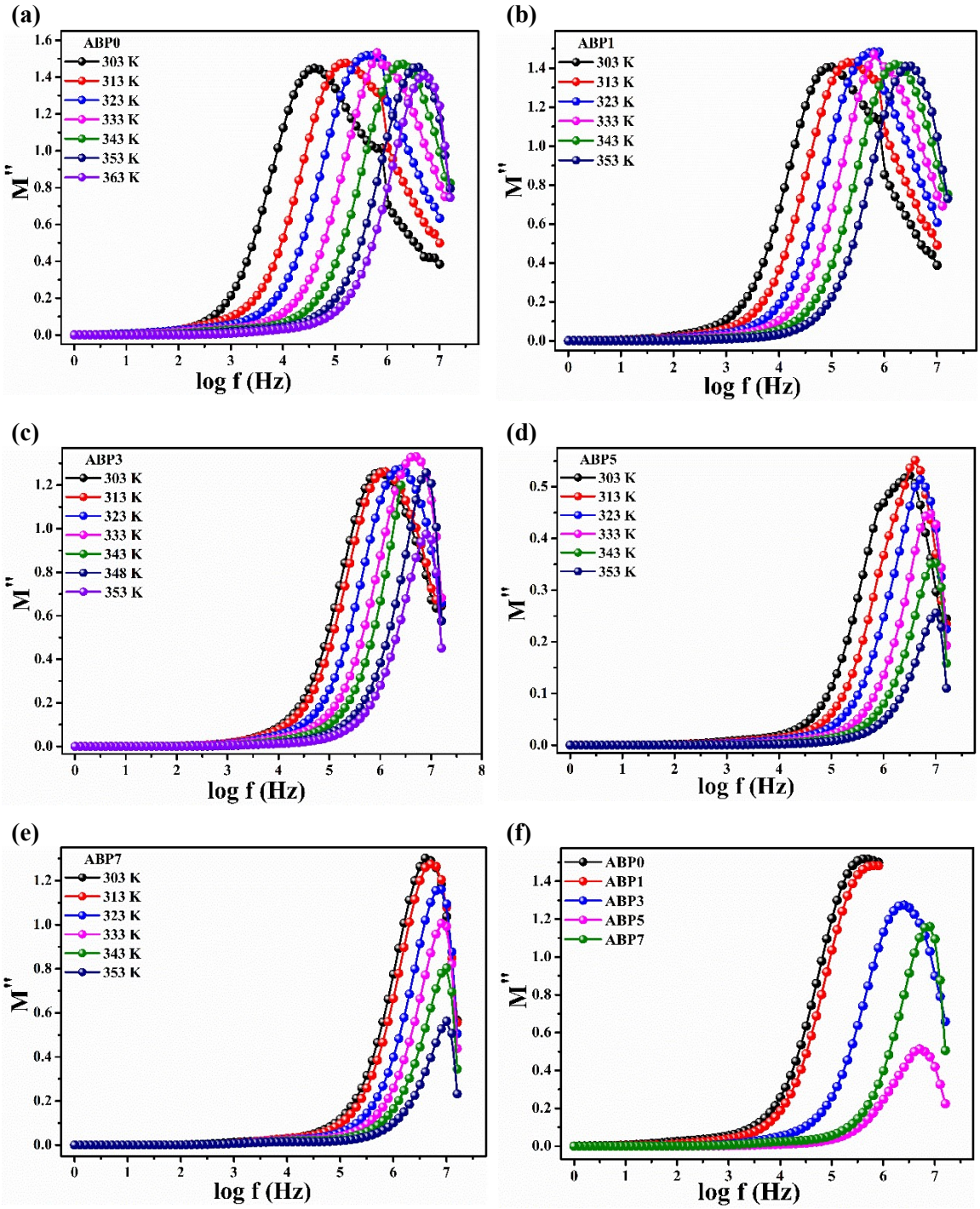


***Figure 6.18:*** *Plots of M" vs. logarithmic function of frequency, (a-d) respectively for ABP0 to ABP7 samples at different temperatures, (f) all the glass samples at 323 K.*

The observed shift of the relaxation peak towards higher frequency with increasing temperature indicates the presence of temperature-dependent relaxation processes in the glass system under investigation. $Ag^+$ ions exhibit long-range mobility in the frequency range below $M''_{max}$, but are restricted to short-range movement in a narrow dimensional potential well in the frequency range above $M''_{max}(f > f_p)$. The peak region indicates the shift from long to short range mobility of ions. Fig. 6.19(a) displays a plot of $M''$and $Z$"

values as a function of frequency. The observed discrepancy between the frequency peaks of $M''$ and $Z$" plots confirms the relaxation process in the glasses studied, which is attributed to the localized movement of charge carriers. The $M''$ data were fitted to the KWW function [71], which is a stretched exponential.

The plot in Fig. 6.19(b) displays the relationship between activation energy for conduction and the stretching parameter [67], [74], while inset shows the trend of stretching parameter ($\beta$) as a function of temperature, which is equivalent to the full width at half maximum (FWHM) of the $M''$ curve, for all of the glass compositions. It exhibits a positive correlation with both temperature and composition. The frequency exponent 'n' does not comply with Ngai's relation, $\beta = 1 - n$, [75], [76] as stated in Eq. 6.11.

The frequency exponent ($n$) is estimated from the high frequency region of the conductivity spectra, and the stretching parameter ($\beta$) is determined between the shoulders of the electric modulus peak. The imperfect fit of the imaginary part of the electric modulus plots at high frequencies impacts the $\beta$ value. The observed variations in the values of $\beta$ and $n$ are consistent with the notion that these parameters reflect ion interaction [77].
Fig. 6.19(c) displays the reciprocal temperature dependence of the modulus relaxation time for all glass compositions, fitting closely to the Arrhenius relation [78]–[80].

$$\tau_c = \tau_0 exp\left(\frac{E_\tau}{K_B T}\right) \quad \ldots\ldots (6.13)$$

The symbol $\tau_c$ represents the characteristic relaxation time, while $\tau_0$ denotes the pre-exponential factor. Additionally, $E_\tau$ signifies the activation energy for $\tau_c$.

The activation energy values obtained from the dc conductivity processes are denoted as $E_\sigma$ and range from $0.84 - 0.52\ eV$, representing the activation energy for long-range charge transport. On the other hand, the activation energy values obtained from the relaxation processes denoted as $E_\tau$, correspond to short-distance transport and range from $0.64 - 0.29\ eV$. These values appear to differ, as illustrated in Fig. 6.19(d).
According to Bhattacharya et al; and Dutta et al; [78], [80], the obtained results indicate that the dc conduction process and the conductivity relaxation processes are activated by distinct mechanisms. In Fig. 6.19(e), the plot against $log\ f$, the relaxation peak of the $M$"spectrum concurs with the corresponding dispersion area in the $M'$ spectra.

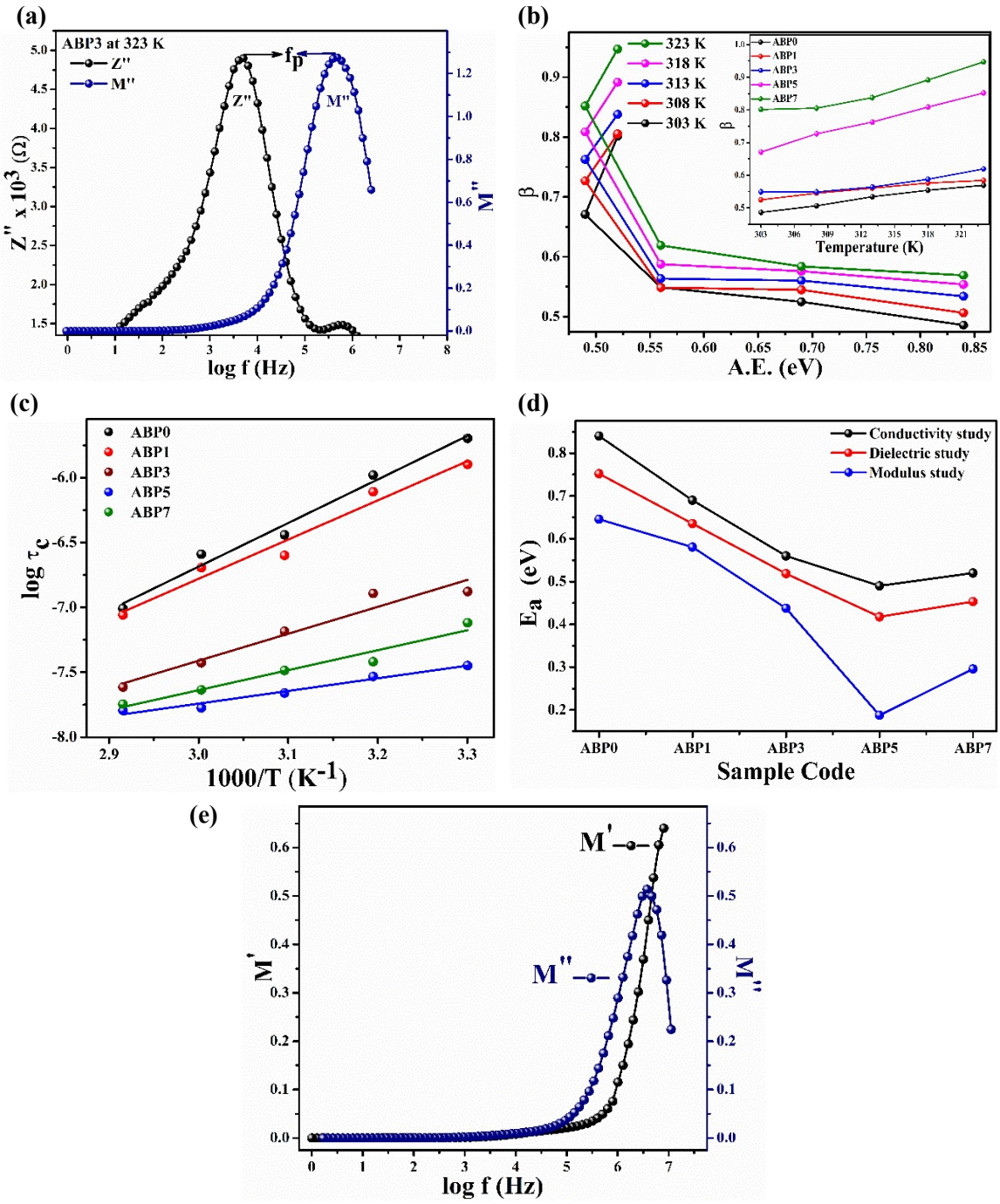


***Figure 6.19***:*(a) Peak of M" and Z" for ABP3 sample at 323 K temperature, (b) β as a function of activation energy at various temperature points, (inset) as a function of temperature for all the glass samples, (c) Modulus relaxation time as a function of reciprocal of temperature- Arrhenius trend for all the glass samples, (d) Activation energy deduced from the conductivity, dielectric and modulus study for all the ABP series samples, (e) The peak of real and imaginary part of modulus as a function of frequency for ABP5 sample at 323 K temperature.*

### Modulus Scaling

To understand the dielectric mechanism [4], [77], [81]–[86], several researchers have proposed scaling modulus spectra. The concept of Ac universality was initially identified by Taylor, who demonstrated that the dielectric loss of various ionic glass compositions could be plotted on a single graph against scaled frequency. Subsequently, Isard [87] renamed Taylor's axis the Taylor-Isard formulation, which involves plotting the dielectric loss against the logarithmic function of the product of frequency $(f)$ and dc conductivity$\sigma_{dc}$ (Eq. 6.14). The constant $C$ exhibits a proportionality relationship with the inverse of temperature.

$$\sigma = \frac{\sigma(\omega)}{\sigma_0} = F\left(c\frac{\omega}{\sigma_0}\right) \quad \ldots\ldots (6.14)$$

AC universality in disordered solids allows for the scaling of frequency-dependent parameter measurements across different temperatures and glass compositions into a single master curve, as demonstrated by various studies [39], [48], [88]–[92]. Summerfield originally proposed a normalized value for the imaginary part of the modulus, which was later modified by Roling [85] to account for scaling with frequency, dc conductivity, temperature, and carrier concentration.

$$\frac{M''}{M_p''} = F\left(\frac{f}{\sigma_{dc}T}\right) \quad \ldots\ldots (6.15)$$

Ghosh [76] proposed the empirical formula for modulus scaling, which involves normalizing both axes by their respective peak values.

$$\frac{M''}{M_p''} = F\left(\frac{f}{f_p}\right) \ldots\ldots (6.16)$$

In the investigation of relaxation mechanisms in ion-conducting materials, such as glasses and polymer systems, the use of scaling aspects has proven to be advantageous. Scaling allows for a more comprehensive understanding of the behavior of these materials by relating various properties and parameters through appropriate functions.

In this particular study, the focus is on scaling the modulus functions ($M'$and $M''$), which represent the real and imaginary parts of the modulus, respectively. To achieve scaling, different models and their corresponding formalisms are being considered: T-I-S (Taylor-Isard-Scaling), Ghosh, Roling, and Summerfield. These models provide frameworks for understanding the relationships between various factors influencing the relaxation mechanisms in ion-conducting materials. In the T-I-S framework, as mentioned in references [65] and [87], the scaling of the actual and imaginary parts of the modulus is

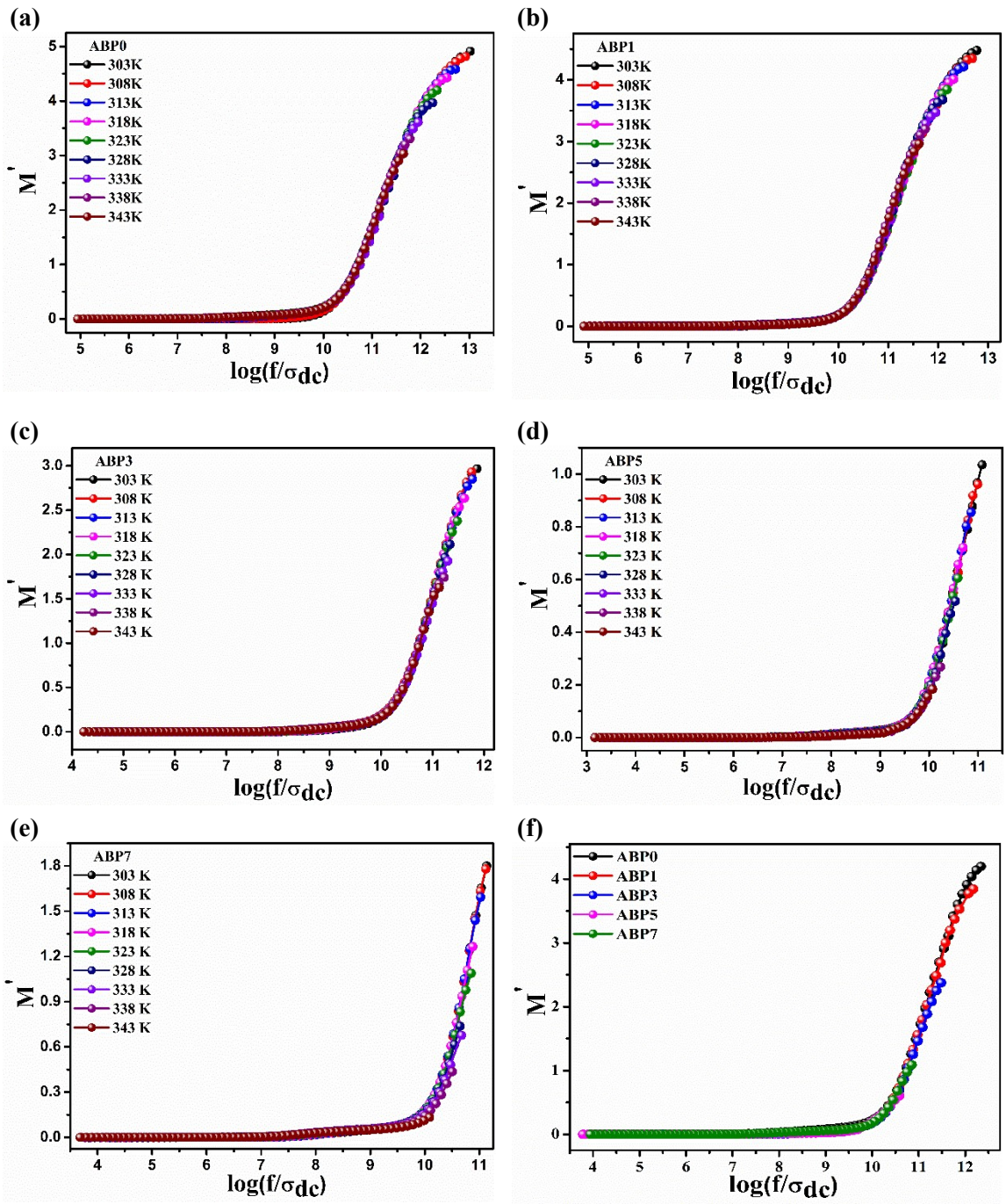


***Figure 6.20:****(a-e)Scaled modulus spectra (M′)plotted against* $log(f/\sigma_{dc})$ *at different temperatures, (f) at 323 K temperature, the real component of modulus(M′) vs the scaled frequency* $log(f/\sigma_{dc})$ *(T-I-S model) for all the glass samples.*

performed with respect to the function $f/\sigma_{dc}$. Here, $f$ represents the frequency of the applied electric field, and $\sigma_{dc}$ represents the direct current (dc) conductivity of the material. By scaling the modulus functions with this ratio, the researchers aim to establish a relationship between the frequency-dependent response and the dc conductivity of the material. In Fig. 6.20 (a-e) of the study, the scaling of $M'$ (real part of the modulus) is depicted as a function of $\log(f/\sigma_{dc})$ for different samples at varying temperatures. This

scaling approach allows for the comparison of the frequency-dependent response of the samples, taking into account the ratio of the applied electric field frequency ($f$) to the direct current conductivity ($\sigma_{dc}$). In Fig. 6.20 (f), the scaling of $M'$ is shown for multiple glass samples at a specific temperature of 323 $K$. This figure provides insights into the behavior of the glass samples and their relaxation mechanisms at that particular temperature. For the $M^{"}$ spectrum (imaginary part of the modulus), additional scaling is performed by considering different x-axis parameters:

- Ghosh model: The $M^{"}$ spectrum is scaled using the normalized frequency ($f/f_p$), where $f_p$ represents the peak frequency. This scaling approach, based on the Ghosh model, allows for a more comprehensive understanding of the relaxation behavior of the material.
- Roling model: The $M^{"}$ spectrum is scaled using the parameter $\log(f/\sigma_{dc}T)$, where $T$ represents temperature. This scaling approach, based on the Roling model, takes into account the combined influence of frequency, dc conductivity, and temperature on the relaxation mechanisms.
- Summerfield model: The $M^{"}$ spectrum, which is scaled using the parameter $\log((f/\sigma_{dc}T)x)$, where x is a scaling factor. This approach, based on the Summerfield model, further extends the understanding of the relaxation behavior by introducing an additional scaling parameter.

In addition, the study attempts to scale the normalized modulus function $M^{"}/M^{"}_{max}$ as a function of its corresponding normalized frequency $f/f_{max}$. This approach, mentioned in references [85] and [93], provides valuable insights into the relative magnitude of the imaginary part of the modulus and its variation with frequency.

Among all the formalisms considered, the study found that the T-I-S, Roling, and Summerfield models resulted in almost successful scaling spectra. These models provided useful frameworks for understanding and characterizing the relaxation mechanisms present in the ion-conducting materials, including glasses and polymer systems.

In Fig. 6.21 (a-b) of the study, the formalism of the T-I-S (Taylor-Isard-Scaling) model is illustrated. This model provides a framework for scaling the modulus functions and relating them to the function $f/\sigma_{dc}$, as mentioned earlier. The figure helps visualize the application of the T-I-S model in the scaling analysis. In Fig. 6.21 (c-d), the scaling based on the Ghosh formalism is demonstrated. The figure provides insights into how the Ghosh model is applied to scale and analyze the behavior of the material.

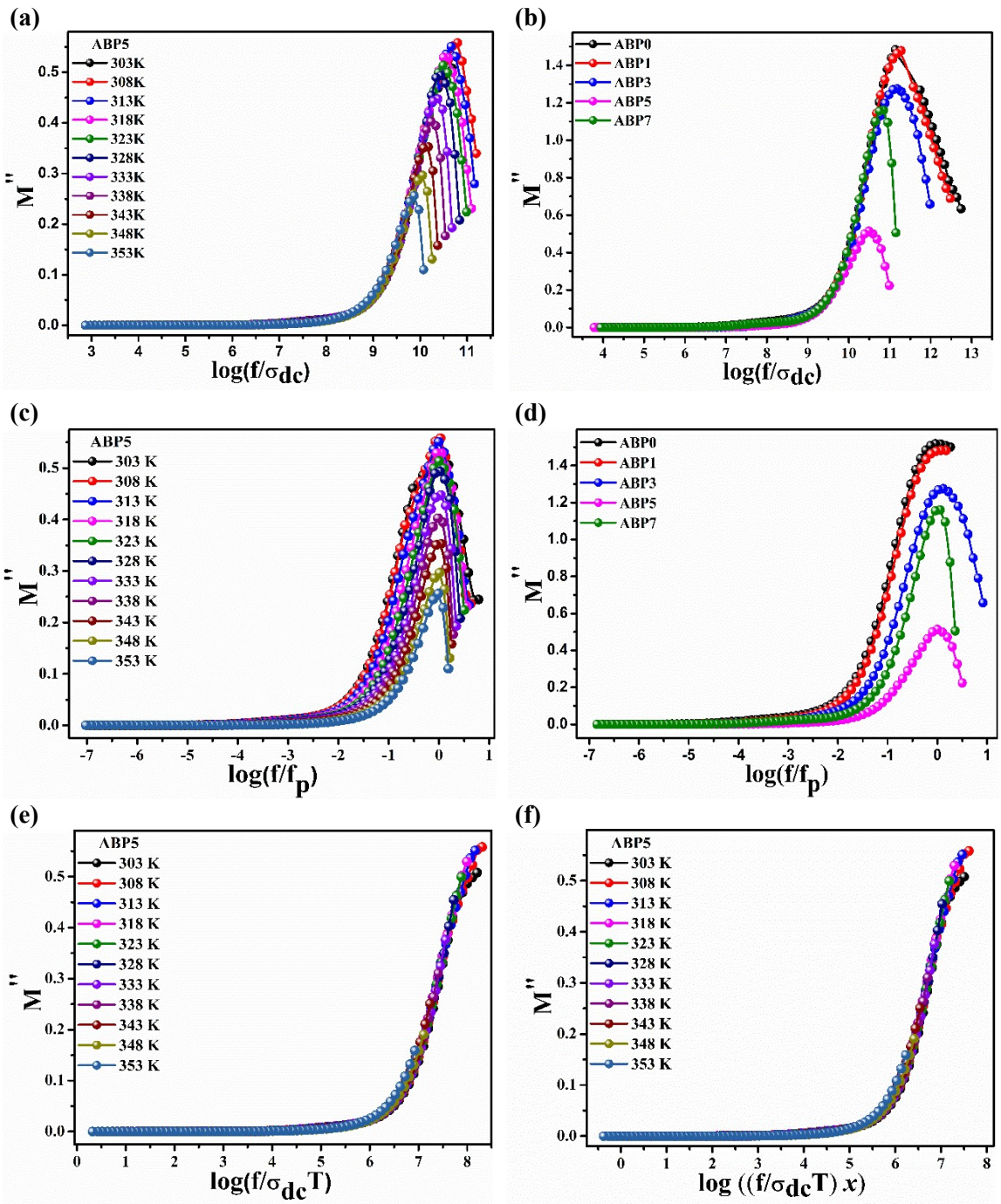


***Figure 6.21**: The imaginary part of modulus ($M^{''}$) is plotted against the scaled frequency by using, (a-b) T-I-S formulation, (c-d) Ghosh formalism, (e) Roling model, and (f) Summerfield model of scaling.*

Fig. 6.21 (e-f) depict the impact of temperature and dopant concentration on scaling, utilizing the Roling and Summerfield models, respectively, for the imaginary part of the modulus function ($M^{''}$). These figures demonstrate how the Roling and Summerfield formalisms are employed to understand the influence of temperature and dopant concentration on the relaxation mechanisms in the material.

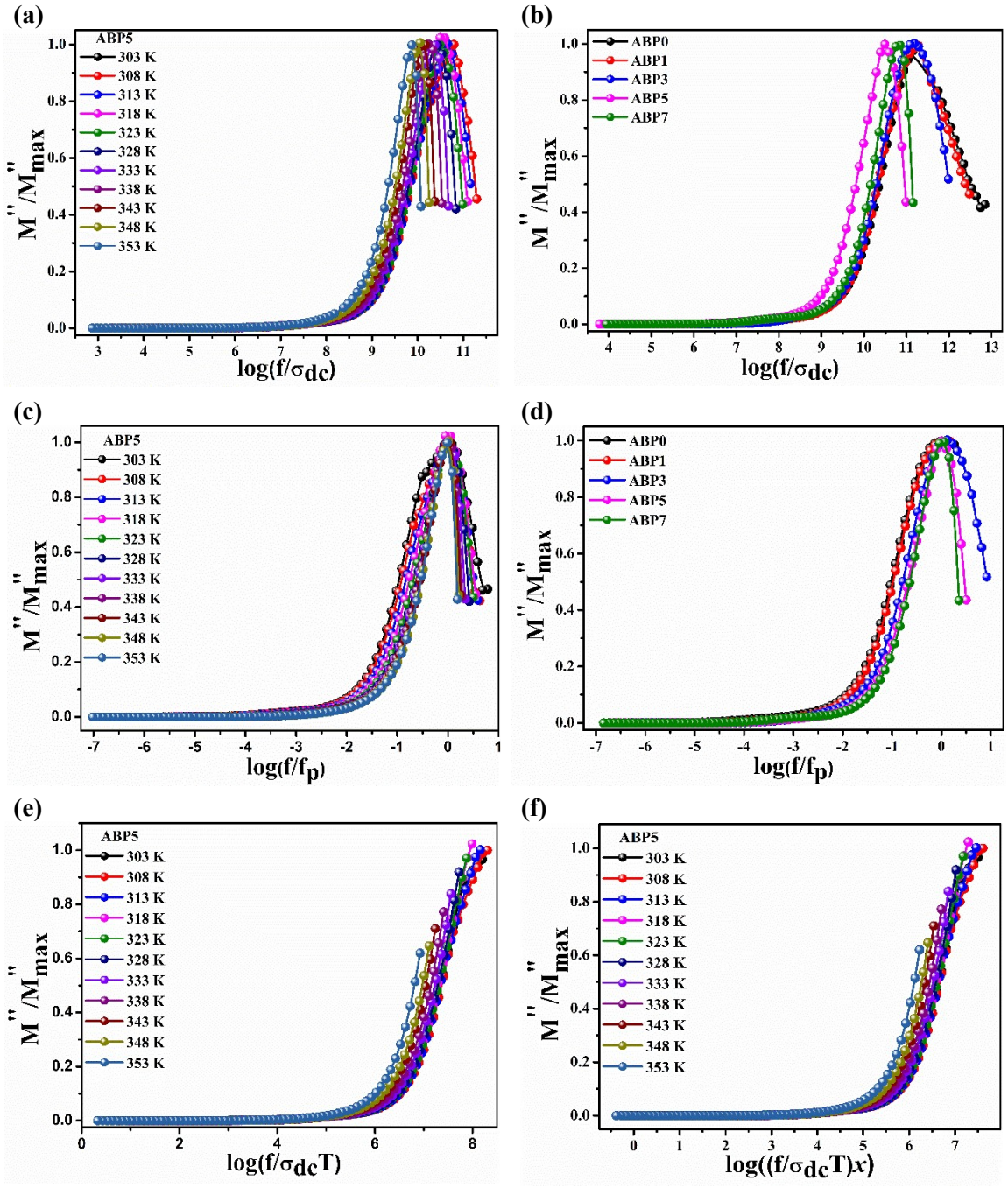


***Figure 6.22**: The normalized modulus function $M^{''}/M^{''}_{max}$ is plotted against the scaled frequency by using, (a-b) T-I-S formulation, (c-d) Ghosh formalism, (e) Roling model, and (f) Summerfield model of scaling.*

Moving on to Fig. 6.22 (a-f), the scaling of the normalized value of the modulus is illustrated as a function of frequency, dc conductivity, normalized frequency, temperature, and salt concentration. These scaling analyses are performed for a specific sample at various temperatures and for all samples at a temperature of $323\,K$. The figures provide a comprehensive understanding of the relationship between these parameters and the behavior of the material. The study suggests that the dynamic processes occurring at

different frequencies are independent of temperature. This conclusion is based on the observation that the modulus curves overlap at all temperatures, indicating a consistent behavior across the temperature range. The integration of the $M'$ and $M''$ spectra into a unified master curve using the T-I-S, Roling, and Summerfield formalisms of scaling, as depicted in Fig. 6.20 (a-f) and 6.21 (e-f), further supports this assertion.

Additionally, the study suggests that the activation energy for all dynamic processes occurring at different time scales is uniform, and temperature does not significantly affect the distribution of relaxation time in the material. This finding implies that the relaxation mechanisms remain consistent despite changes in temperature, providing valuable insights into the underlying behavior of ion-conducting materials.

Based on the observed information, there are several key observations and implications regarding the behavior of dynamic processes in the system under study:

(a) Constant Activation Energy: The data suggests that the activation energy, which is the energy barrier that needs to be overcome for a dynamic process to occur, remains constant across different time scales. This implies that the underlying mechanism driving these processes does not change significantly with time.

(b) Temperature Independence: The distribution of relaxation times, which refers to the timescales associated with the relaxation of certain properties in the system, is not affected by temperature. This suggests that the mechanism of ionic relaxation, at least in the context of the studied system, is not influenced by temperature. Alternatively, this behavior could indicate that the principle of Time Temperature Superposition (TTS) holds, which allows for the prediction of material behavior at different temperatures based on data obtained at a reference temperature.

(c) Unified Master Curve: The data obtained at various temperatures can be integrated into a single master curve. This implies that there is a common underlying behavior governing the dynamic processes across different temperatures. The $M'$ curve scaling, which refers to the real part of the modulus, shows this integration, indicating that the measured property exhibits a consistent response across different temperatures.

(d) Dispersion in Imaginary Modulus: Unlike the real part of the modulus, the imaginary part of the modulus (as observed in Fig. 21(b-d) and Fig. 22(b-d)) does not collapse into a single master curve, particularly in the dispersive frequency region. This suggests

that the behavior of the system at higher frequencies differs from that at lower and mid frequencies.

(e) Composition Independence: The observed master curves for the lower and mid frequency regions, regardless of the specific glass composition, imply that the conductivity relaxation in the system is independent of the composition of the glass. This suggests that the underlying dynamic processes associated with conductivity relaxation are not influenced by changes in the glass composition.

Overall, these findings suggest that the dynamic processes in the studied system exhibit consistent behavior across different time scales, temperatures, and glass compositions, except for the higher frequency range where some differences are observed. The constant activation energy and distribution of relaxation times indicate a certain level of robustness and independence of these processes from external factors, providing valuable insights into the fundamental behavior of the system.

## 6.4 Conclusion

The provided information describes the investigation of ionic conductivity in a vitreous electrolyte system composed of $x(AgI):(100-\mathrm{x})[30Ag_2O:(56B_2O_3+14P_2O_5)]$ glass framework, where $x$ represents the weight percentage of $AgI$. Here are the key findings: The addition of $AgI$ up to 5 $wt.\%$ in the ABP glass series leads to a significant increase in ionic conductivity. The maximum ionic conductivity achieved is $6.24\text{x}10^{-5}$ S/cm at room temperature. This suggests that $AgI$ plays a crucial role in facilitating the migration of $Ag^+$ ions within the glass structure, resulting in enhanced ionic conductivity.

- The temperature-dependent ion conduction mechanism in the borophosphate glass system follows the Anderson-Stuart (A-S) model. The A-S model describes the temperature dependence of ion conduction, which suggests that the mobility of $Ag^+$ ions increases with temperature.
- The frequency-dependent ion migration in the glass system is illustrated by the Jump Relaxation Model. This model implies that the movement of $Ag^+$ ions occurs in a stepwise manner, with jumps between energy minima. The frequency-dependent behavior suggests that the dynamics of ion migration are influenced by the frequency of the applied electric field.
- The investigation of the electric modulus confirms that the relaxation time is distributed, indicating that multiple relaxation processes occur in the vitreous

electrolytes. This suggests that the glass system exhibits a complex dynamic behavior, with various timescales associated with the relaxation of different properties.

- The values of the stretching parameter ($\beta$) indicate a deviation from the ideal Debye nature of relaxation processes. This implies that the relaxation behavior in the vitreous electrolytes is non-Debye, indicating more complex relaxation dynamics than those described by the Debye model.
- The scaling analysis confirms that dynamic processes occurring at different time scales have slightly different activation energies. This indicates that the underlying mechanisms driving these processes may vary slightly depending on the timescale. Additionally, the distribution of relaxation times is found to be independent of both temperature and glass composition, suggesting that it is a characteristic intrinsic to the vitreous electrolyte system.

## Bibliography

[1] A. Magistris, G. Chiodelli, and M. Duclot, "Silver borophosphate glasses : Ion transport, thermal stability and electrochemical behaviour," *Solid State Ionics*, vol. 9–10, no. PART 1, pp. 611–615, 1983, doi: 10.1016/0167-2738(83)90303-X.

[2] K.J. Rao, *Structural Chemistry of Glasses*. Elsevier, 2002. doi: 10.1016/B978-0-08-043958-7.X5017-1.

[3] P. Boolchand and W. J. Bresser, "Mobile silver ions and glass formation in solid electrolytes," *Nature*, vol. 410, no. 6832, pp. 1070–1073, Apr. 2001, doi: 10.1038/35074049.

[4] D. D. Ramteke and R. S. Gedam, "Study of Li2O-B2O3-Dy2O 3 glasses by impedance spectroscopy," *Solid State Ionics*, vol. 258, pp. 82–87, May 2014, doi: 10.1016/j.ssi.2014.02.006.

[5] D. D. Ramteke, H. C. Swart, and R. S. Gedam, "Electrochemical response of Nd 3+ ions containing lithium borate glasses," *J. Rare Earths*, vol. 35, no. 5, pp. 480–484, May 2017, doi: 10.1016/S1002-0721(17)60937-2.

[6] J. Mizerakova, P. Hockicko, and F. Munoz, "Dielectric Study of Lithium and Sodium Borophosphate Glasses," *Commun. - Sci. Lett. Univ. Zilina*, vol. 19, no. 3, pp. 46–50, Sep. 2017, doi: 10.26552/com.C.2017.3.46-50.

[7] D. Larink, H. Eckert, M. Reichert, and S. W. Martin, "Mixed network former effect in ion-conducting alkali borophosphate glasses: Structure/property correlations in the system [M2O] 1/3[(B2O3)x(P2O 5)1- X]2/3 (M = Li, K, Cs)," *J. Phys. Chem. C*, vol. 116, no. 50, 2012, doi: 10.1021/jp307085t.

[8] R. Suresh Kumar and K. Hariharan, "AC conductivity and electrical relaxation studies on 10CuI-60AgI-30V2O5 glasses," *Mater. Chem. Phys.*, vol. 60, no. 1, pp. 28–38, Jul. 1999, doi: 10.1016/S0254-0584(99)00057-7.

[9] K. Funke *et al.*, "Low-temperature α-AgI confined in glass: Structure and dynamics," *Solid State Ionics*, vol. 271, pp. 2–9, 2015, doi: 10.1016/j.ssi.2014.09.033.

[10] H. Iwahara, "Conducting Materials: Solid-ionic and Super-ionic," Elsevier, 2001. doi: 10.1016/b0-08-043152-6/00269-2.

[11] V. K. Deshpande, "Science and technology of glassy solid electrolytes," in *IOP Conference Series: Materials Science and Engineering*, 2009, vol. 2. doi: 10.1088/1757-899X/2/1/012011.

[12] in: W. V. G. (Ed. . D. Kunze, "Fast Ion Transport in Solids," *North-Holland, Amsterdam, Netherlands,* pp. 405–411, 1973.

[13] S. Hoshino, "REVIEW Structure and dynamics of solid state ionics SOLID STATE IONICS," 1991.

[14] T. Minami, Y. Ikeda, and M. Tanaka, "Infrared spectra, glass transition temperature, and conductivity of superionic conducting glasses in the systems AgXAg2OB2O3 (X = I, Br)," *J. Non. Cryst. Solids*, vol. 52, no. 1–3, pp. 159–169, Dec. 1982, doi: 10.1016/0022-3093(82)90290-3.

[15] P. Sharma, D. K. Kanchan, M. Pant, M. S. Jayswal, and N. Gondaliya, "Effect of AgI on Conduction Mechanism in Silver-Vanadate Superionic Glasses," *New J. Glas. Ceram.*, vol. 01, no. 03, pp. 112–118, 2011, doi: 10.4236/njgc.2011.13016.

[16] V. A. Adhwaryu and D. K. Kanchan, "Effect of Lithium Iodide on transport phenomenon in Lithium Borophosphate glass Electrolyte," *J. Non. Cryst. Solids*, vol. 583, p. 121474, May 2022, doi: 10.1016/J.JNONCRYSOL.2022.121474.

[17] F. S. Howell, R. A. Bose, P. B. Macedo, and C. T. Moynihan, "Electrical Relaxation in a Glass-Forming Molten Salt."

[18] C. A. Angell, *MOBILE IONS IN AMORPHOUS SOLIDS*, vol. 43, no. 1. Annual Reviews, 1992, pp. 693–717. doi: 10.1146/annurev.physchem.43.1.693.

[19] James E Shelby, *Introduction to Glass Science and Technology*, 2nd ed. Royal Society of Chemistry, 2015.

[20] M. Htut, M. Lwin, P. Kaung, and S. Htoon, *No Title*, vol. IV, no. 2. 2006. http://www.iaea.org/inis/collection/NCLCollectionStore/_Public/40/057/40057374.

[21] C. Gautam, A. K. Yadav, and A. K. Singh, "A Review on Infrared Spectroscopy of Borate Glasses with Effects of Different Additives," *ISRN Ceram.*, vol. 2012, pp. 1–17, 2012, doi: 10.5402/2012/428497.

[22] S. Kabi and A. Ghosh, *Mixed glass former effect in AgI doped silver borophosphate glasses*, vol. 262. Elsevier, p. 778−781. doi: 10.1016/j.ssi.2013.09.028.

[23] P. N. Rao, E. Ramesh Kumar, and B. Appa Rao, *Structural and transport studies of CdI2−doped silver borotellurite fast ion−conducting system*, vol. 22, no. 12. Ionics, p. 3863−3871. doi: 10.1007/s10008−018−4094−9.

[24] V. N. Rai, B. N. Raja Sekhar, D. M. Phase, and S. K. Deb, "EFFECT OF GAMMA IRRADIATION ON THE STRUCTURE AND VALENCE STATE OF Nd IN

PHOSPHATE GLASS."

[25] H. A. Othman, H. S. Elkholy, and I. Z. Hager, "FTIR of binary lead borate glass: Structural investigation," *J. Mol. Struct.*, vol. 1106, pp. 286–290, Feb. 2016, doi: 10.1016/j.molstruc.2015.10.076.

[26] Y. M. Lai, X. F. Liang, S. Y. Yang, J. X. Wang, L. H. Cao, and B. Dai, "Raman and FTIR spectra of iron phosphate glasses containing cerium," *J. Mol. Struct.*, vol. 992, no. 1–3, pp. 84–88, Apr. 2011, doi: 10.1016/j.molstruc.2011.02.049.

[27] A. M. Efimov, "IR fundamental spectra and structure of pyrophosphate glasses along the 2ZnO · P2O5-2Me2O · P2O5 join (Me being Na and Li)," *J. Non. Cryst. Solids*, vol. 209, no. 3, pp. 209–226, 1997, doi: 10.1016/S0022-3093(96)00562-5.

[28] J. J. Hudgens and S. W. Martin, *Mid-IR and far-IR investigation of AgI-doped silver diborate glasses*, vol. 53, no. 9. 1996, pp. 5348–5355. doi: 10.1103/PhysRevB.53.5348.

[29] S. Kabi and A. Ghosh, "Mixed glass former effect in AgI doped silver borophosphate glasses," *Solid State Ionics*, vol. 262, pp. 778–781, Sep. 2014, doi: 10.1016/j.ssi.2013.09.028.

[30] L. Balachander, G. Ramadevudu, M. Shareefuddin, R. Sayanna, and Y. C. Venudharc, "IR analysis of borate glasses containing three alkali oxides," *ScienceAsia*, vol. 39, no. 3, pp. 278–283, Jun. 2013, doi: 10.2306/scienceasia1513-1874.2013.39.278.

[31] R. C. Agrawal and R. K. Gupta, "Superionic solids: composite electrolyte phase - an overview," *J. Mater. Sci.*, vol. 34, no. 6, pp. 1131–1162, Jan. 1999, doi: 10.1023/A:1004598902146.

[32] K. J. Hamam and F. Salman, "Dielectric constant and electrical study of solid-state electrolyte lithium phosphate glasses," *Appl. Phys. A*, vol. 125, no. 9, p. 621, Sep. 2019, doi: 10.1007/s00339-019-2868-2.

[33] K. Srinivas, P. Sarah, and S. V. Suryanarayana, "Impedance spectroscopy study of polycrystalline Bi6Fe2Ti3O18," *Bull. Mater. Sci.*, vol. 26, no. 2, pp. 247–253, 2003, doi: 10.1007/BF02707799.

[34] A. Pan and A. Ghosh, *Activation energy and conductivity relaxation of sodium tellurite glasses*, vol. 59, no. 2. 1999, pp. 899–904. doi: 10.1103/PhysRevB.59.899.

[35] W. Wang, R. Christensen, B. Curtis, S. W. Martin, and J. Kieffer, "A new model linking elastic properties and ionic conductivity of mixed network former glasses," *Phys. Chem. Chem. Phys.*, vol. 20, no. 3, pp. 1629–1641, 2018, doi: 10.1039/c7cp04534d.

[36] M. Luis *et al.*, *No Title*, vol. 35. Sociedade Brasileira de Fisica, 2005, pp. 626–631. doi: 10.1590/S0103-97332005000400007.

[37] O. L. ANDERSON and D. A. STUART, "Calculation of Activation Energy of Ionic Conductivity in Silica Glasses by Classical Methods," *J. Am. Ceram. Soc.*, vol. 37, no. 12, pp. 573–580, Dec. 1954, doi: 10.1111/j.1151-2916.1954.tb13991.x.

[38] S E Anderson and R S Drago, "The CBH model was introduced by Pike to account for the dielectric loss in scandium oxide.," *Phys. Rev. B*, vol. 6, p. 1527, 1972.

[39] C. A. Angell, "Dynamic processes in ionic glasses," *Chem. Rev.*, vol. 90, no. 3, pp. 523–542, May 1990, doi: 10.1021/cr00101a006.

[40] K. J. Hamam *et al.*, "Temperature and frequency effect on the electrical properties of bulk nickel phthalocyanine octacarboxylic acid (Ni-Pc(COOH)8)," *Appl. Phys. A*, vol. 125, no. 1, p. 7, Jan. 2019, doi: 10.1007/s00339-018-2147-7.

[41] N. Chakchouk, B. Louati, and K. Guidara, "Electrical properties and conduction mechanism study by OLPT model of NaZnPO4 compound," *Mater. Res. Bull.*, vol. 99, pp. 52–60, Mar. 2018, doi: 10.1016/j.materresbull.2017.10.046.

[42] M. Dult, R. S. Kundu, S. Murugavel, R. Punia, and N. Kishore, "Conduction mechanism in bismuth silicate glasses containing titanium," *Phys. B Condens. Matter*, vol. 452, pp. 102–107, Nov. 2014, doi: 10.1016/j.physb.2014.07.004.

[43] S. Murugavel and M. Upadhyay, "A.C. conduction in amorphous semiconductors," *J. Indian Inst. Sci.*, vol. 91, p. 303, 2011.

[44] K. Funke, "Debye-Hückel-Type Relaxation Processes in Solid Ionic Conductors," *Zeitschrift für Phys. Chemie*, vol. 154, no. 1–2, pp. 251–295, Jan. 1987, doi: 10.1524/zpch.1987.154.Part_1_2.251.

[45] K. Funke, "Jump relaxation in solid ionic conductors," *Solid State Ionics*, vol. 28–30, no. PART 1, pp. 100–107, 1988, doi: 10.1016/S0167-2738(88)80015-8.

[46] D. P. Almond, "COMMENTS ON THE ANALYSES OF AC CONDUCTIVITY DATA FOR SINGLE CRYSTAL Na P-ALUMINA AT LOW TEMPERATURES Their fits gave values for," Elsevier Sequoia S.A, 1985.

[47] S. Summerfield, "Universal low-frequency behaviour in the a.c. hopping conductivity of disordered systems," *Philos. Mag. B Phys. Condens. Matter; Stat. Mech. Electron. Opt. Magn. Prop.*, vol. 52, no. 1, pp. 9–22, 1985, doi: 10.1080/13642818508243162.

[48] B. Roling, A. Happe, K. Funke, and M. D. Ingram, "Carrier Concentrations and Relaxation

Spectroscopy: New Information from Scaling Properties of Conductivity Spectra in Ionically Conducting Glasses," *Phys. Rev. Lett.*, vol. 78, no. 11, pp. 2160–2163, Mar. 1997, doi: 10.1103/PhysRevLett.78.2160.

[49] A. Ghosh and A. Pan, *Scaling of the conductivity spectra in ionic glasses: Dependence on the structure*, vol. 84, no. 10. 2000, pp. 2188–2190. doi: 10.1103/PhysRevLett.84.2188.

[50] J. C. Dyre, P. Maass, B. Roling, and D. L. Sidebottom, "Fundamental questions relating to ion conduction in disordered solids," *Reports Prog. Phys.*, vol. 72, no. 4, 2009, doi: 10.1088/0034-4885/72/4/046501.

[51] I. Svare, *Conductivity and NMR relaxation from ionic motion in disordered glasses with distributions of barriers*, vol. 125, no. 1. Elsevier Science Publishers B.V., 1999, pp. 47–53. doi: 10.1016/S0167-2738(99)00157-5.

[52] M. Vogel, C. Brinkmann, H. Eckert, and A. Heuer, "Origin of nonexponential relaxation in a crystalline ionic conductor: A multidimensional 109Ag NMR study," *Phys. Rev. B - Condens. Matter Mater. Phys.*, vol. 69, no. 9, 2004, doi: 10.1103/PhysRevB.69.094302.

[53] D. L. Sidebottom, "Colloquium: Understanding ion motion in disordered solids from impedance spectroscopy scaling," *Rev. Mod. Phys.*, vol. 81, no. 3, pp. 999–1014, Aug. 2009, doi: 10.1103/RevModPhys.81.999.

[54] J. Ilic, "Wood: Electrical Properties," in *Encyclopedia of Materials: Science and Technology*, Elsevier, 2001, pp. 9629–9633. doi: 10.1016/B0-08-043152-6/01744-7.

[55] D. L. Sidebottom, B. Roling, and K. Funke, "Ionic conduction in solids: Comparing conductivity and modulus representations with regard to scaling properties," *Phys. Rev. B*, vol. 63, no. 2, p. 024301, Dec. 2000, doi: 10.1103/PhysRevB.63.024301.

[56] R. Kaushik, K. Hariharan, and S. Radhakrishna, "Transport studies on thin films of Ag7I4VO4 solid electrolyte," *J. Appl. Electrochem.*, vol. 17, no. 4, pp. 813–820, Jul. 1987, doi: 10.1007/BF01007819.

[57] Chowdari B V R and Radhakrishna S, "Materials for Solid State Batteries," 1986.

[58] B. V. . Chowdari and K. Radhakrishnan, "Electrical and electrochemical characterization of Li2O:P2O5:Nb2O5-based solid electrolytes," *J. Non. Cryst. Solids*, vol. 110, no. 1, pp. 101–110, Jul. 1989, doi: 10.1016/0022-3093(89)90187-7.

[59] R. D. Armstrong and K. Taylor, "The impedance of solid electrolyte cells over the frequency range 10−3 to 108 Hz," *J. Electroanal. Chem. Interfacial Electrochem.*, vol. 63, no. 1, pp. 9–17, Jul. 1975, doi: 10.1016/S0022-0728(75)80121-5.

[60] J. M. Stevels, “The Electrical Properties of Glass,” 1957, pp. 350–391. doi: 10.1007/978-3-642-45859-0_3.

[61] E. Barsoukov and J. R. Macdonald, Eds., *Impedance Spectroscopy*. Wiley, 2005. doi: 10.1002/0471716243.

[62] M. Venkateswarlu, “A.c. conductivity and dielectric studies of silver-based fast ion conducting glass system,” *Solid State Ionics*, vol. 127, no. 1–2, pp. 177–184, Jan. 2000, doi: 10.1016/S0167-2738(99)00257-X.

[63] S. A. SUTHANTHIRARAJ and S. RADHAKRISHNA, “Transport studies on thin films of Ag6I4MoO4 solid electrolyte,” *Cryst. lattice defects Amorph. Mater.*, vol. 11, no. 3, pp. 185–195, 1985.

[64] B. CHOWDARI and R. GOPALAKRISHNAN, “Impedance and modulus spectroscopy of vitreous AgI□Ag2O□P2O5 system,” *Solid State Ionics*, vol. 18–19, pp. 483–487, Jan. 1986, doi: 10.1016/0167-2738(86)90164-5.

[65] J. C. Dyre and T. B. Schrøder, “Universality of ac conduction in disordered solids,” *Rev. Mod. Phys.*, 2000, doi: 10.1103/RevModPhys.72.873.

[66] D. L. Sidebottom and J. Zhang, *Scaling of the ac permittivity in ion-conducting glasses*, vol. 62, no. 9. 2000, pp. 5503–5507. doi: 10.1103/PhysRevB.62.5503.

[67] H. K. Patel and S. W. Martin, *No Title*, vol. 45, no. 18. 1992, pp. 10292–10300. doi: 10.1103/PhysRevB.45.10292.

[68] D. Sidebottom, P. Green, and R. Brow, “Scaling parallels in the non-Debye dielectric relaxation of ionic glasses and dipolar supercooled liquids,” *Phys. Rev. B - Condens. Matter Mater. Phys.*, vol. 56, no. 1, pp. 170–177, 1997, doi: 10.1103/PhysRevB.56.170.

[69] H. Kumar Patel and H. Kumar, “Impedance spectroscopy and NMR studies of fast ion conducting chalcogenide glasses Recommended Citation.” [Online]. Available: https://lib.dr.iastate.edu/rtd/10850

[70] D. L. Sidebottom, P. F. Green, and R. K. Brow, *Comparison of KWW and power law analyses of an ion-conducting glass*, vol. 183, no. 1–2. 1995, pp. 151–160. doi: 10.1016/0022-3093(94)00587-7.

[71] C. T. Moynihan, “Analysis of electrical relaxation in glasses and melts with large concentrations of mobile ions,” Sep. 1994. doi: 10.1016/0022-3093(94)90668-8.

[72] K. L. Ngai and O. Kanert, *No Title*, vol. 53–56, no. PART 2. 1992, pp. 936–946. doi: 10.1016/0167-2738(92)90275-T.

[73] M. S. Jayswal, D. K. Kanchan, P. Sharma, and N. Gondaliya, "Relaxation process in PbI2-Ag2O-V2O 5-B2O3 system: Dielectric, AC conductivity and modulus studies," *Mater. Sci. Eng. B Solid-State Mater. Adv. Technol.*, vol. 178, no. 11, pp. 775–784, Jun. 2013, doi: 10.1016/j.mseb.2013.03.013.

[74] S. W. Martin, "Conductivity relaxation in glass: Compositional contributions to non-exponentiality," *Appl. Phys. A Solids Surfaces*, vol. 49, no. 3, pp. 239–247, Sep. 1989, doi: 10.1007/BF00616850.

[75] K. L. Ngai, J. N. Mundy, H. Jain, O. Kanert, and G. Balzer-Jollenbeck, "Correlation between the activation enthalpy and Kohlrausch exponent for ionic conductivity in alkali aluminogermanate glasses," *Phys. Rev. B*, vol. 39, no. 9, pp. 6169–6179, Mar. 1989, doi: 10.1103/PhysRevB.39.6169.

[76] A. Pan and A. Ghosh, *Relaxation dynamics of lithium ions in lead bismuthate glasses*, vol. 62, no. 5. 2000, pp. 3190–3195. doi: 10.1103/PhysRevB.62.3190.

[77] K. L. Ngai, G. N. Greaves, and C. T. Moynihan, *No Title*, vol. 80, no. 5. 1998, pp. 1018–1021. doi: 10.1103/PhysRevLett.80.1018.

[78] S. Bhattacharya and A. Ghosh, "ac relaxation in silver vanadate glasses," *Phys. Rev. B*, vol. 68, no. 22, p. 224202, Dec. 2003, doi: 10.1103/PhysRevB.68.224202.

[79] S. Bhattacharya and A. Ghosh, "Relaxation of silver ions in fast ion conducting molybdate glasses," *Solid State Ionics*, vol. 176, no. 13–14, 2005, doi: 10.1016/j.ssi.2005.03.002.

[80] A. Dutta and A. Ghosh, "Ionic conductivity of Li2O–BaO–Bi2O3 glasses," *J. Non. Cryst. Solids*, vol. 351, no. 3, pp. 203–208, Feb. 2005, doi: 10.1016/j.jnoncrysol.2004.11.010.

[81] K. Ngai and R. Rendell, "Interpreting the real part of the dielectric permittivity contributed by mobile ions in ionically conducting materials," *Phys. Rev. B - Condens. Matter Mater. Phys.*, vol. 61, no. 14, pp. 9393–9398, 2000, doi: 10.1103/PhysRevB.61.9393.

[82] M. D. Ingram, "Ionic conductivity and glass structure," *Philos. Mag. B Phys. Condens. Matter; Stat. Mech. Electron. Opt. Magn. Prop.*, vol. 60, no. 6, pp. 729–740, 1989, doi: 10.1080/13642818908209739.

[83] A. S. Nowick and B. S. Lim, "Analysis of ac conductivity data for Na2O·3SiO2 glass by stretched exponential and Jonscher power-law methods," *J. Non. Cryst. Solids*, vol. 172–174, no. 2, pp. 1389–1394, Sep. 1994, doi: 10.1016/0022-3093(94)90667-X.

[84] J. M. Bobe, J. M. Réau, J. Senegas, and M. Poulain, "F- ion conductivity and diffusion properties in ZrF4-based fluoride glasses with various NaF concentrations (0 ≤ xNaF ≤

0.45)," *Solid State Ionics*, vol. 82, no. 1–2, pp. 39–52, Nov. 1995, doi: 10.1016/0167-2738(95)00192-9.

[85] B. Roling, *What do electrical conductivity and electrical modulus spectra tell us about the mechanisms of ion transport processes in melts, glasses, and crystals?*, vol. 244, no. 1. Elsevier, 1999, pp. 34–43. doi: 10.1016/S0022-3093(98)00847-3.

[86] N. H. Vasoya, P. K. Jha, K. G. Saija, S. N. Dolia, K. B. Zankat, and K. B. Modi, "Electric Modulus, Scaling and Modeling of Dielectric Properties for Mn2+-Si4+ Co-substituted Mn-Zn Ferrites," *J. Electron. Mater.*, vol. 45, no. 2, pp. 917–927, Feb. 2016, doi: 10.1007/s11664-015-4224-4.

[87] J. O. Isard, "A study of the migration loss in glass and a generalized method of calculating the rise of dielectric loss with temperature," *Proc. IEE - Part B Electron. Commun. Eng.*, vol. 109, no. 22S, pp. 440–447, 1962, doi: 10.1049/pi-b-2.1962.0077.

[88] S. R. Elliott and A. P. Owens, "The diffusion-controlled relaxation model for ionic transport in glasses," *Philos. Mag. B*, vol. 60, no. 6, pp. 777–792, Dec. 1989, doi: 10.1080/13642818908209742.

[89] M. T. M. Y. J.M. Hyde, *Phys. Chem. Glas.*, vol. 28, p. 174, 1987.

[90] H. Kahnt, "Ionic Transport in Oxide Glasses and Frequency Dependence of Conductivity," *Berichte der Bunsengesellschaft für Phys. Chemie*, vol. 95, no. 9, pp. 1021–1025, Sep. 1991, doi: 10.1002/bbpc.19910950913.

[91] M. Sural and A. Ghosh, "Conductivity relaxation in zirconium fluoride glasses: effect of substitution of Zr4+ by Y3+ ions," *Solid State Ionics*, vol. 120, no. 1–4, pp. 27–32, May 1999, doi: 10.1016/S0167-2738(98)00551-7.

[92] J. O. Isard, "Dielectric dispersion in amorphous conductors," *J. Non. Cryst. Solids*, vol. 4, pp. 357–365, Apr. 1970, doi: 10.1016/0022-3093(70)90063-3.

[93] T. B. Schrøder and J. C. Dyre,"Scaling and universality of ac conduction in disordered solids," *Phys. Rev. Lett.*, vol.84, no. 2, pp. 310–313, 2000, doi: 10.1103/PhysRevLett.84.310.